Cellular/Molecular

The mTOR Substrate S6 Kinase 1 (S6K1) Is a Negative Regulator of Axon Regeneration and a Potential Drug Target for Central Nervous System Injury

Hassan Al-Ali,[1,2,3]* Ying Ding,[5,6]* Tatiana Slepak,[1]* Wei Wu,[5] Yan Sun,[5,7] Yania Martinez,[1] Xiao-Ming Xu,[5] Vance P. Lemmon,[1,3] and John L. Bixby[1,3,4]

[1]Miami Project to Cure Paralysis, University of Miami Miller School of Medicine, Miami, Florida 33136, [2]Peggy and Harold Katz Family Drug Discovery Center, University of Miami Miller School of Medicine, Miami, Florida 33136, [3]Department of Neurological Surgery, University of Miami Miller School of Medicine, Miami, Florida 33136, [4]Department of Molecular and Cellular Pharmacology, University of Miami Miller School of Medicine, Miami, Florida 33136, [5]Spinal Cord and Brain Injury Research Group, Stark Neurosciences Research Institute, Department of Neurological Surgery, Indiana University School of Medicine, Indianapolis, Indiana 46202, [6]Department of Histology and Embryology, Zhongshan School of Medicine, Sun Yat-sen University, Guangzhou, Guangdong 510080, China, and [7]Department of Anatomy, Histology and Embryology, School of Basic Medical Sciences, Fudan University, Shanghai, 200032, China

The mammalian target of rapamycin (mTOR) positively regulates axon growth in the mammalian central nervous system (CNS). Although axon regeneration and functional recovery from CNS injuries are typically limited, knockdown or deletion of PTEN, a negative regulator of mTOR, increases mTOR activity and induces robust axon growth and regeneration. It has been suggested that inhibition of S6 kinase 1 (S6K1, gene symbol: RPS6KB1), a prominent mTOR target, would blunt mTOR's positive effect on axon growth. In contrast to this expectation, we demonstrate that inhibition of S6K1 in CNS neurons promotes neurite outgrowth *in vitro* by twofold to threefold. Biochemical analysis revealed that an mTOR-dependent induction of PI3K signaling is involved in mediating this effect of S6K1 inhibition. Importantly, treating female mice *in vivo* with PF-4708671, a selective S6K1 inhibitor, stimulated corticospinal tract regeneration across a dorsal spinal hemisection between the cervical 5 and 6 cord segments (C5/C6), increasing axon counts for at least 3 mm beyond the injury site at 8 weeks after injury. Concomitantly, treatment with PF-4708671 produced significant locomotor recovery. Pharmacological targeting of S6K1 may therefore constitute an attractive strategy for promoting axon regeneration following CNS injury, especially given that S6K1 inhibitors are being assessed in clinical trials for nononcological indications.

Key words: axon regeneration; drug discovery; drug target; kinase; S6K; spinal cord injury

Significance Statement

Despite mTOR's well-established function in promoting axon regeneration, the role of its downstream target, S6 kinase 1 (S6K1), has been unclear. We used cellular assays with primary neurons to demonstrate that S6K1 is a negative regulator of neurite outgrowth, and a spinal cord injury model to show that it is a viable pharmacological target for inducing axon regeneration. We provide mechanistic evidence that S6K1's negative feedback to PI3K signaling is involved in axon growth inhibition, and show that phosphorylation of S6K1 is a more appropriate regeneration indicator than is S6 phosphorylation.

Introduction

The PI3K/mammalian target of rapamycin (mTOR) pathway is a key regulator of axon growth and regeneration in the CNS (Park et al., 2008). Typically, axons in the adult mammalian CNS have limited capacity for regeneration following injury. Activating the PI3K/mTOR pathway by knockdown or genetic deletion of its negative regulator, PTEN, results in a marked increase in regenerative capacity (Zerhouni, 2004; Park et al., 2008, 2010; Zukor et

Received April 4, 2017; revised May 18, 2017; accepted May 27, 2017.

Author contributions: H.A., Y.D., T.S., W.W., Y.S., X.-M.X., V.P.L., and J.L.B. designed research; H.A., Y.D., T.S., W.W., Y.S., and Y.M. performed research; H.A., Y.D., and T.S. analyzed data; H.A., T.S., X.-M.X., V.P.L., and J.L.B. wrote the paper.

This work was supported by Department of Defense Grant W81XWH-13–1-077 and the National Institutes of Health Grant HD057632 to J.L.B. and V.P.L., and National Institutes of Health Grant NS059622, Department of Defense Grant CDMRP W81XWH-12-1-0562, U.S. Department of Veterans Affairs Merit Review Award I01 BX002356, and Craig H. Neilsen Foundation 296749 to X.-M.X., V.P.L. holds the Walter G. Ross Distinguished Chair in Developmental Neuroscience. X.-M.X. holds the Mari Hulman George Chair in Neurological Surgery. We thank Yan Shi for help with cell imaging and high content analysis.

The authors declare no competing financial interests.

*H.A., Y.D., and T.S. contributed equally to this work as co-first authors.

Correspondence should be addressed to either of the following: Dr. John L. Bixby, University of Miami Miller School of Medicine, 1400 NW 10th Avenue, DT 1205, Miami, FL 33136, E-mail: jbixby@med.miami.edu; or Dr. Vance P. Lemmon, University of Miami Miller School of Medicine, 1095 NW 15th Terrace, LPLC 4-16, Miami, FL 33136, E-mail: vlemmon@med.miami.edu.

DOI:10.1523/JNEUROSCI.0931-17.2017

 0270-6474/17/377079-17$15.00/0

al., 2013), and mTOR activity is critical for the regeneration induced by loss of PTEN (Park et al., 2010). The mechanisms through which mTOR promotes axon growth/regeneration are less clear; in particular, the role(s) of S6K1, a downstream effector of mTOR, are incompletely understood (Hubert et al., 2014; Yang et al., 2014).

We previously screened a large number of kinase inhibitors in a neurite outgrowth assay using primary hippocampal neurons, and identified "hit" compounds that promote neurite outgrowth (Al-Ali et al., 2013b). This phenotypic assay is reliable (Z' factor > 0.7) and has identified both chemical and genetic perturbagens that promote axon growth from a variety of CNS neurons (Al-Ali et al., 2013a, 2017). In a follow-up study, we used machine learning to relate data from the phenotypic screen of kinase inhibitors to kinase profiling data, which allowed us to identify (and verify) "target" kinases whose inhibition induces neurite outgrowth (Al-Ali et al., 2015). These target kinases included representatives of the family of ribosomal S6 protein kinases (RPS6Ks).

Two types of S6 kinases have been described based on their domain topology: the p70 ribosomal S6 kinases (S6K1 and S6K2, which phosphorylate S6 at $S^{235/236/240/244/247}$) and the p90 ribosomal S6 kinases (RSK1, RSK2, RSK3, and RSK4, which phosphorylate S6 at $S^{235/236}$) (Meyuhas, 2015). Two additional p90 kinases, MSK1 and MSK2, are included in the family by virtue of sequence similarity (Pearce et al., 2010b) but do not appear to have substantial activity toward S6. Previous studies have shown that RSKs and MSKs negatively regulate neurite outgrowth (Loh et al., 2008; Fischer et al., 2009; Buchser et al., 2010; Hubert et al., 2014). Therefore, the finding that their inhibition promotes neurite outgrowth might be expected. The observation that neuronal S6K1 activity may be negatively correlated with neurite outgrowth was interesting, however, given the well-established role of its upstream activator mTOR as a positive regulator of axon growth.

In dividing cells, S6K1 acts as a negative feedback regulator of the PI3K/mTOR pathway, such that inhibition of S6K1 leads to induction of PI3K signaling and subsequent activation of mTOR (Pende et al., 2004; Um et al., 2004; Magnuson et al., 2012). In this study, we show that a similar regulatory mechanism occurs in neurons: inhibition of S6K1 induces neurite outgrowth in an mTOR-dependent manner. Importantly, we demonstrate that treating mice with a selective S6K1 inhibitor following transection of the corticospinal tract (CST) promoted robust CST axonal regeneration across and beyond the lesion site. This regeneration was accompanied by improved behavioral recovery, suggesting that axon regeneration induced by S6K1 inhibition may be helpful in recovery from CNS injury.

Materials and Methods

Antibodies, reagents, and compounds. Pan Akt (#2920), pT^{308}Akt (#4056), pS^{473}Akt (#4058), pan S6 ribosomal protein (#2317), $pS^{240/244}$S6 (#5364), pan S6K1 (#2708), and pT^{389}S6K1 (#9205) antibodies (working dilution 1:1000, except for S6 pan, which was diluted 1:300) were purchased from Cell Signaling Technology. GAPDH (#IMG-5019A-1) antibody (working dilution 1:500) was purchased from Imgenex. βIII-tubulin (#T2200) antibody (working dilution 1:2000) was purchased from Sigma-Aldrich. Alexa fluorophore-conjugated secondary antibodies (working dilution 1:1000) were purchased form Invitrogen. IRDye-700- and IRDye-800-conjugated secondary antibodies (working dilutions 1:15000) were purchased from LiCor. Poly-D-lysine (P7886-500MG) and sterile DMSO (D2650) were purchased from Sigma-Aldrich. Hippocampal tissue was incubated in Hibernate E (without calcium) from BrainBits, supplemented with NeuroCult SM1 (05711) from Stem Cell Technologies. Neurons were cultured in NbActive4 media from BrainBits. Accell siRNAs (working concentration 1 μM) were purchased from GE Healthcare/Dharmacon (scramble SMARTPool #D-001910-10-20, S6K1 siRNA SMARTPool #E-099323-00-0003, scramble oligo #D-001910-04-05, S6 set of 4 siRNA oligos #EU-089542-00-0002). Kinase inhibitors PF-4708671, ML-7, ROCK inhibitor IV, IKK inhibitor VII, Flt3 inhibitor III, and Bisindolylmaleimide I, and rapamycin were purchased from EMD Millipore. GW784684X, GW659386A, GSK1511931A, GSK269962B, and SB-750140 were acquired via collaboration from GlaxoSmithKline. RO0480500-002 was acquired via collaboration from Roche. VCC379989:02 and VCC781016:01 were purchased from Vichem. Torin-2 was purchased from Tocris Bioscience. All other reagents were purchased from Invitrogen.

Neurite outgrowth assay for small-molecule kinase inhibitors. The neurite outgrowth assay was performed as previously described (Al-Ali et al., 2013b), with minor modifications. Briefly, compounds were tested with rat embryonic (E18) hippocampal neurons cultured at low density for 48 h. Neurons were plated at 1500–1800 cells/well in 96-well plates coated overnight with poly-D-lysine. For the pretreatment condition, mTOR inhibitors were added to the cells 1 h before the addition of S6K1 inhibitor. Plates were fixed, immunostained, and imaged in a Cellomics ArrayScan VTI. Images were automatically traced using the Neuronal Profiling Bioapplication (version 3.5). Data were analyzed using MATLAB (R2014b, MathWorks).

Neurite outgrowth assay for siRNAs. Dissociated hippocampal neurons were seeded in 96-well poly-D-lysine-coated plates at 1500–1800 cells per well in 150 μl of NbActive4 and incubated overnight. The following day, siRNA solutions were prepared in 96-well plates at 2 μM in 100 μl of media and allowed to equilibrate for 1 h in a CO_2 incubator. Immediately before treatment, 100 μl of media was removed from the cells and replaced with 50 μl of siRNA solution (duplicate wells for each treatment) to bring the final siRNA reagent concentration to 1 μM (per vendor recommendation) in a total volume of 100 μl. Cells were incubated for 96 h, then fixed and analyzed for neurite outgrowth as previously described for the neurite outgrowth assay (Al-Ali et al., 2013b).

Assessing protein phosphorylation. Hippocampal (E18) neurons were cultured in NbActive4 (Invitrogen). Cells were seeded into 24-well plates at $0.25–0.5 \times 10^6$ cells/well in 0.5 ml of media. Compound stocks (10 mM in DMSO) were diluted in cell culture media at 2× final concentration and added at 1:1 volume to cells (final volume = 1 ml). Control wells received the corresponding volume of DMSO, which was kept constant across all treatments at 0.2% v/v. Each plate contained two DMSO control wells (one normalization control and one treatment control). After indicated time points, cells were washed once with PBS and collected in 120 μl of lysis buffer containing 100 mM Tris-HCl, pH 6.8, 20% glycerol, 4% SDS, 5% β-mercaptoethanol, phosphatase inhibitor mixture (Clontech), protease inhibitor mixture (Roche), and 0.2% bromophenol blue. Lysates were boiled for 5–7 min, and 20 μl of each sample was loaded on a 10% polyacrylamide gel. Protein was transferred from the gel to a nitrocellulose membrane in a wet transfer apparatus using 25 mM sodium bicarbonate as transferring solution. Membranes were blocked with Odyssey blocking buffer for at least 1 h, then incubated overnight in primary antibody solution (1:1 PBS, Odyssey blocking buffer with 0.1% Tween 20) at 4°C on a shaker. Membranes were washed 3× in PBS-Tween (10 min washes) and incubated in secondary antibody solution (secondary antibodies in 1:1 PBS, Odyssey blocking buffer with 0.1% Tween and 0.02% SDS) at room temperature for 2 h with shaking. The 800-IR-dye-conjugated secondary antibodies were used to develop total protein bands, and the 680-IR-dye-conjugated secondary antibodies were used to develop phosphorylated protein bands. Finally, membranes were washed 5× in PBS Tween (10 min washes). Blots were scanned using an Odyssey system. Relative change in phosphorylation in response to treatment was computed as follows:

$$\text{Change in phosphorylation} = \frac{\text{Sample 700 signal}}{\text{Sample 800 signal}} \Big/ \frac{\text{control 700 signal}}{\text{control 800 signal}} \quad (1)$$

Assessing target protein knockdown. Neurons were plated in 48-well plates at $\sim 0.25 \times 10^6$ cells/well and transfected with siRNAs at 1 μM in a

total volume of 200 μl. Three days following transfection, cells were lysed and analyzed by SDS-PAGE followed by Western blotting as above.

Assessing S6 mRNA knockdown. Neurons were plated in 48-well plates at ~0.25×10^6 cells/well and transfected with siRNAs at 1 μM in a total volume of 200 μl. One day following transfection, RNA was isolated from the neurons using the micro RNAeasy (QIAGEN, #74004) kit. Total amount of isolated RNA was quantified using a NanoDrop 1000 (NanoDrop Products). Reverse transcription (RT) reaction was performed using the Advantage RT PCR kit (Clontech) with 1 μg of isolated RNA and both oligo dT and random hexamer primers. Samples were collected from two independent experiments and qPCR for each sample was set up in triplicates using the Power SYBR Green PCR Master Mix (Applied Biosystems) according to manufacturer suggestions. Controls included a No-RT control to ensure absence of contaminating DNA, cDNA plasmid control (1 pg/ml) to verify the correct product size, and qPCR of GAPDH and β-actin housekeeping genes for normalization. Reactions were run on 7300 RealTime PCR System (Applied Biosystems), and the results were analyzed using Sequence Detection System version 1.2.3 (Applied Biosystems) software.

Animal studies. A total of 30 adult C57BL/6 mice (7 weeks, Harlan Laboratories) were used in the *in vivo* studies. Only female mice were used because males often get bladder infections and develop kidney problems after this kind of spinal cord injury. All behavior testing, surgical interventions, and postoperative animal care were performed in accordance with the *Guide for the care and use of laboratory animals* (National Research Council) and were approved by the Indiana University Institutional Animal Care and Use Committee. The mice were pretrained for behavior analysis for 4 weeks before the surgery (see Fig. 8*A*). Two mice were unable to learn the task and were excluded from the experiment. The remaining 28 animals received dorsal hemisection surgery at the end of the pretraining and baseline behavioral testing.

Spinal cord dorsal hemisection and cortical injection of PF-4708671. At the 10th week of age (4 weeks after training), mice (20–30 g) were anesthetized with an intraperitoneal injection of a ketamine/xylazine/acepromazine mixture (120 mg/3.3 mg/1.67 mg /kg) provided by Laboratory Animal Resource Center at Indiana University School of Medicine, Indianapolis. Mice were then subjected to stabilization of the C5/C6 vertebra with a vertebral stabilizer. After the exposure of the C5-C6 dorsal laminae, a transverse durotomy at the interlaminar space between C5 and C6 was performed using a 30 G needle followed by cutting with a pair of microscissors. A midline dorsal hemisection was performed using a VibraKnife attached to the Louisville Injury System Apparatus (Louisville Impactor System, Louisville, KY) according to a previously published method (Sivasankaran et al., 2004; Y. Liu et al., 2008; Zhang et al., 2013) with modifications. Briefly, the blade was 1.2 mm wide and was advanced 0.9 mm ventrally from the dorsal surface of the cord, extending beyond the central canal (see Fig. 1*B*). Such a lesion completely transected the entire dorsal corticospinal tract (dCST) and lateral corticospinal tract (lCST) on both sides. In the C57BL/6 mice, we did not observe the presence of the ventral CST (vCST). Thus, a dorsal hemisection in our model (1.2 mm wide, 0.9 mm deep) transected all descending CST axons at the lesion site. In this case, any labeled CST axons growing beyond the lesion would be interpreted as coming from cut axons via either regeneration from the tips or by regenerative sprouting.

Compounds were injected bilaterally into sensorimotor cortex after the C5-C6 dorsal hemisection according to a previously established method (Wang et al., 2014). Briefly, after the dorsal hemisection, animals were randomly assigned into four groups that receive the following cortical injections ($n = 7$/group): Group 1 (control): DMSO (0.1% DMSO in 0.1 M PBS); Group 2 (low-dose PF): 1 mM PF-4708671 (in 0.1% DMSO in 0.1 M PBS); Group 3 (medium-dose PF-4708671): 5 mM PF-4708671 (in 0.1% DMSO in 0.1 M PBS); and Group 4 (high-dose): 10 mM PF-4708671 (in 0.1% DMSO in 0.1 M PBS). Five stereotaxic injections of PF-4708671 were made into the sensorimotor cortex on each side at a depth of 0.5 mm and coordination of 2 mm/1.5 mm, 1.25 mm/1.5 mm, 0.5 mm/1.5 mm, −0.25 mm/1 mm, and −1 mm/1 mm (anteroposterior/mediolateral to the bregma) with 1 μl/injection site. After the surgery and PF-4708671 injections, an analgesic agent, buprenorphine, was given intraperitoneally every 12 h for 2 d (Laboratory Animal Resource Center, Indiana University, Indianapolis).

Single-pellet reaching task. The single-pellet reaching task is a simple repetitive training protocol used to test the precise and coordinated motor movements of the forelimb. The single-pellet reaching task was performed in accordance with a previously described method (Chen et al., 2014). In this test, a clear Plexiglas training chamber (15 cm long × 8.5 cm wide × 20 cm tall) contains three vertical slits (one slit on "shaping" edge and two slits on the opposite "training" edge). The vertical slits are 0.5 cm wide and 13 cm tall and are located on the front wall of the box: in the center, on the left side, and on the right side. A food platform (8.5 cm long × 4.4 cm wide × 0.9 cm tall) is placed in the front side (facing the trainer) of the training chamber during training sessions. There are two divot slots on the food platform for positioning seeds: one slot on the left and the other slot on the right side. The divots are 0.3 cm from the long edge and 2.4 cm from the width edge (Chen et al., 2014). The left and right divot slots correspond to the left and right slits in the mouse training chamber and are used for training of dominant forelimbs. The purpose of having these divot slots is to ensure that the pellet (millet seed) is placed consistently at the same place for each reaching attempt. The training phase contained food deprivation (2 d), shaping (7 d), and training (9 d). The mice were trained for 30 reaching attempts on the preferred limb for 20 min per day. Reaching behavior and scoring were recorded according to the following four categories: (1) Success: The mouse reaches with preferred paw, grasps and retrieves the seed, and feeds it into its mouth. Success (%) = (the number of success/total number of feeding seeds) × 100. (2) Grasp: The mouse reaches with preferred paw, grasps the seed, but drops it before putting it into its mouth. Grasp (%) = (the number of grasp/total number of feeding seeds) × 100. (3) Reach: The mouse reaches with preferred paw toward the seed, but it either misses the seed or knocks it off from the holding plate. Reach (%) = (the number of reach/total number of feeding seeds) × 100. (4) No reach: The mouse attempts to grasp the seed, but it cannot reach the seed in the holding plate. No reach (%) = (the number of no reach/total number of feeding seeds) × 100. In all mice, a baseline task was performed at 3 d before the surgery. The single-pellet reaching task was also assessed at 1, 2, 4, and 6 weeks after the dorsal hemisection and PF-4708671 treatment (see Fig. 8*A*).

Rotarod test. The Rotarod test was used to assess motor coordination in rodents following procedures described previously with minor modification (N. K. Liu et al., 2013). Briefly, mice were placed on a rotating rod (diameter 30 mm) in a 5-lane Rotarod device (IITC Life Science) that accelerated from 0 to 30 rpm within a 90 s period, with each trial lasting a maximum of 120 s. Trials ended when the animal either fell off the rod or clung to the rod as it made one complete rotation. The animals were trained five times per day for 3 d. The Rotarod tests were performed before injury to score the baseline latencies for each animal. The baseline value was scored as the mean of five trials at 3 d before surgery (see Fig. 1*A*). The Rotarod test was performed at 1, 2, 4, and 6 weeks after the surgery. Data were expressed as the ratio of duration relative to baseline.

Adhesive removal test. Animals were trained for the adhesive removal test for 3 d, and the baseline was recorded at 3 d before the dorsal hemisection (see Fig. 8*A*) according to a protocol previously described (Bouet et al., 2009; N. K. Liu et al., 2013). This concise sensorimotor function assay was performed by applying adhesive tape on the forepaw of the animal and measuring the time to contact and the time to remove it. A 3 mm × 4 mm adhesive tape strip (waterproof adhesive tape, ACME/Chaston) was, respectively, pressed on the left and right sides of the forepaw covering the whole palm and proximal part of the digits. The time to contact and time to remove the adhesive tape were collected with a maximum of 3 min/animal. The time to contact is defined as the point at which the mouse reacts to the affected paw by either shaking its paw or bringing the paw to its mouth. The time to remove is the point when the tape is removed by its mouth, combined with assistance from the forelimb in loosening it. The adhesive removal test was also assessed at 1, 2, 4, and 6 weeks after the dorsal hemisection (see Fig. 8*A*).

Grid-walking test. The grid-walking test assesses the ability to place the forepaws on the rungs of a grid accurately during spontaneous exploration. The mice were trained to walk on a wire grid (0.35 m long with 10 mm squares) for 3 d according to an established protocol with modifications (N. K. Liu et al., 2013). The percentage of forepaw drops below the grid plane during a 3 min observation period was calculated at 3 d before

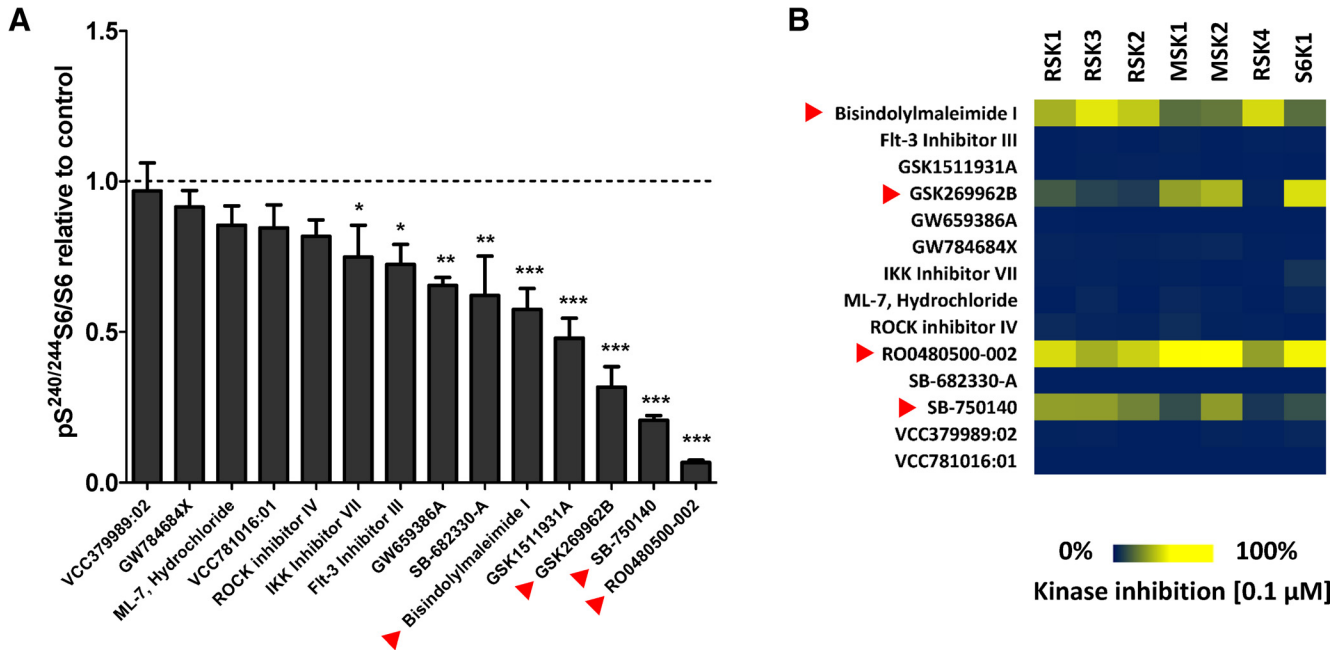

Figure 1. Ribosomal S6 protein phosphorylation is reduced by most kinase inhibitors that promote neurite outgrowth in primary hippocampal neurons. ***A***, Fourteen small-molecule kinase inhibitors were selected, from a set of neurite outgrowth-promoting compounds, to represent distinct chemical scaffolds and diverse kinase activity profiles (Al-Ali et al., 2015). Neurons were treated with the compounds at 1 μM (or DMSO vehicle as a control) for 10 h before lysis and analysis by Western blotting. Most compounds (9 of 14) resulted in significantly reduced S6 phosphorylation (relative to DMSO control) at Serine $^{240/244}$, the substrate site for S6K1, and four others exhibited a trend toward reduced S6 phosphorylation. Data are mean ± SEM. $n = 4$ experimental replicates from two separate preparations of primary neurons. *$p < 0.05$ (one-way ANOVA with Dunnett's multiple comparisons test). **$p < 0.01$ (one-way ANOVA with Dunnett's multiple comparisons test). ***$p < 0.001$ (one-way ANOVA with Dunnett's multiple comparisons test). ***B***, In vitro kinase activity assays for RSK1 (RPS6KA1), RSK3 (RPS6KA2), RSK2 (RPS6KA3), MSK1 (RPS6KA5), MSK2 (RPS6KA4), RSK4 (RPS6KA6), and S6K1 (RPS6KB1) with the 14 representative compounds. Increasing inhibition is indicated by increased intensity of yellow. Only four of the compounds directly inhibited catalytic activity of S6 kinases *in vitro* (red arrowheads).

surgery (as a baseline) and at 1, 2, 4, and 6 weeks after the dorsal hemisection (see Fig. 8*A*).

Anterograde tracing with biotinylated-dextran amine. Six weeks after the dorsal hemisection, mice received bilateral injections of biotinylated-dextran amine (BDA, 10,000 MW, 10% in saline; Invitrogen) into the sensorimotor cortex to trace the CST axons anterogradely. Five injections of BDA (0.5 μl/each) were made into the sensorimotor cortex on each side using the same coordinates as the PF-4708671 injection. For each injection, 0.5 μl of BDA was delivered for a period of 5 min via a glass pipette attached to a 10 μl syringe connected to the Stoelting motorized integrated stereotaxic injectors system (Stoelting). Mice were humanely killed by a lethal dose of anesthesia and transcardially perfused with saline followed by 4% PFA 2 weeks after the BDA injection (see Fig. 1*A*).

BDA visualization and immunofluorescent labeling. After perfusion, the spinal cords containing the lesion epicenter were removed and postfixed in 4% PFA overnight, and were then equilibrated in 30% sucrose for cryoprotection. Sagittal sections at 25 μm were cut using a cryostat. BDA-labeled CST axons were visualized by using avidin-biotin peroxidase incubation followed by biotinyl tyramide and Extra-Avidin-FITC (SAT700, PerkinElmer) (Wang et al., 2014). Lesion gaps were identified in the same sections by immunostaining for GFAP (1:1000; Millipore). Quantification of BDA-labeled CST axons was performed with the experimenter blind to the treatment groups. Briefly, 7 sagittal sections of the spinal cord spaced 125 μm apart were chosen. The middle section was defined as the one that cut through the central canal (see Fig. 3*A*). The other 6 sections were selected at 125, 250, and 375 μm lateral to the middle section on each side. The number of BDA-immunoreactive (IR) CST axon fragments was counted at defined zones spaced 0.5 mm apart. The axon numbers were converted into CST Axon Index defined as a ratio of the BDA-IR axon number at a given zone over the total number of BDA-IR axons in the dCST on a cross section of the C1 spinal cord. The lesion epicenter on the sagittal section is defined as "0 mm," and all other zones are defined as their distances from the lesion epicenter.

Statistical and computational analyses. All computational analyses and tools were implemented in MATLAB (R2013b and R2014b, MathWorks). Statistical analyses were performed in GraphPad Prism (5.03), MATLAB, or Excel (2007). Data were presented as mean ± SEM, unless otherwise noted. Statistical analyses were performed using the GraphPad Software (Prism 5.0) with ANOVA followed by the appropriate post-test correction, or two-way repeated-measures ANOVA with Bonferroni post-test. Statistical significance was accepted with $p < 0.05$.

Results

Phosphorylation of ribosomal S6 protein is reduced by kinase inhibitors that promote neurite outgrowth

A set of small-molecule kinase inhibitors was selected from the hits in our phenotypic screen to represent a variety of chemical scaffolds, distinct kinase inhibition profiles, and potentially diverse mechanisms for promoting neurite outgrowth (Al-Ali et al., 2013b, 2015). In the present study, we investigated the effect of these representative compounds on S6 phosphorylation, in primary hippocampal neurons. We observed that the majority (9 of 14) of these compounds induced a significant reduction in S6 phosphorylation at S $^{240/244}$ (Fig. 1*A*), sites phosphorylated exclusively by S6K1/2 (Pende et al., 2004). Interestingly, only 4 of the 14 compounds directly inhibit S6 kinase activity in enzymatic assays *in vitro* (Fig. 1*B*). This finding suggests that some of the compounds reduce S6K1 phosphorylation of S6 without directly inhibiting the enzyme.

Highly selective S6K1 inhibitor promotes neurite outgrowth

Because the catalytic kinase domains of S6 kinases are structurally similar, most inhibitors of one S6 kinase tend to inhibit other kinases within the S6 kinase family (Fig. 1*B*). One compound (PF-4708671), however, has unusual selectivity for S6K1, both within the group of S6 kinases (Pearce et al., 2010a) and across the kinome (Fig. 2*A*). PF-4708671 was shown to inhibit S6K1 with

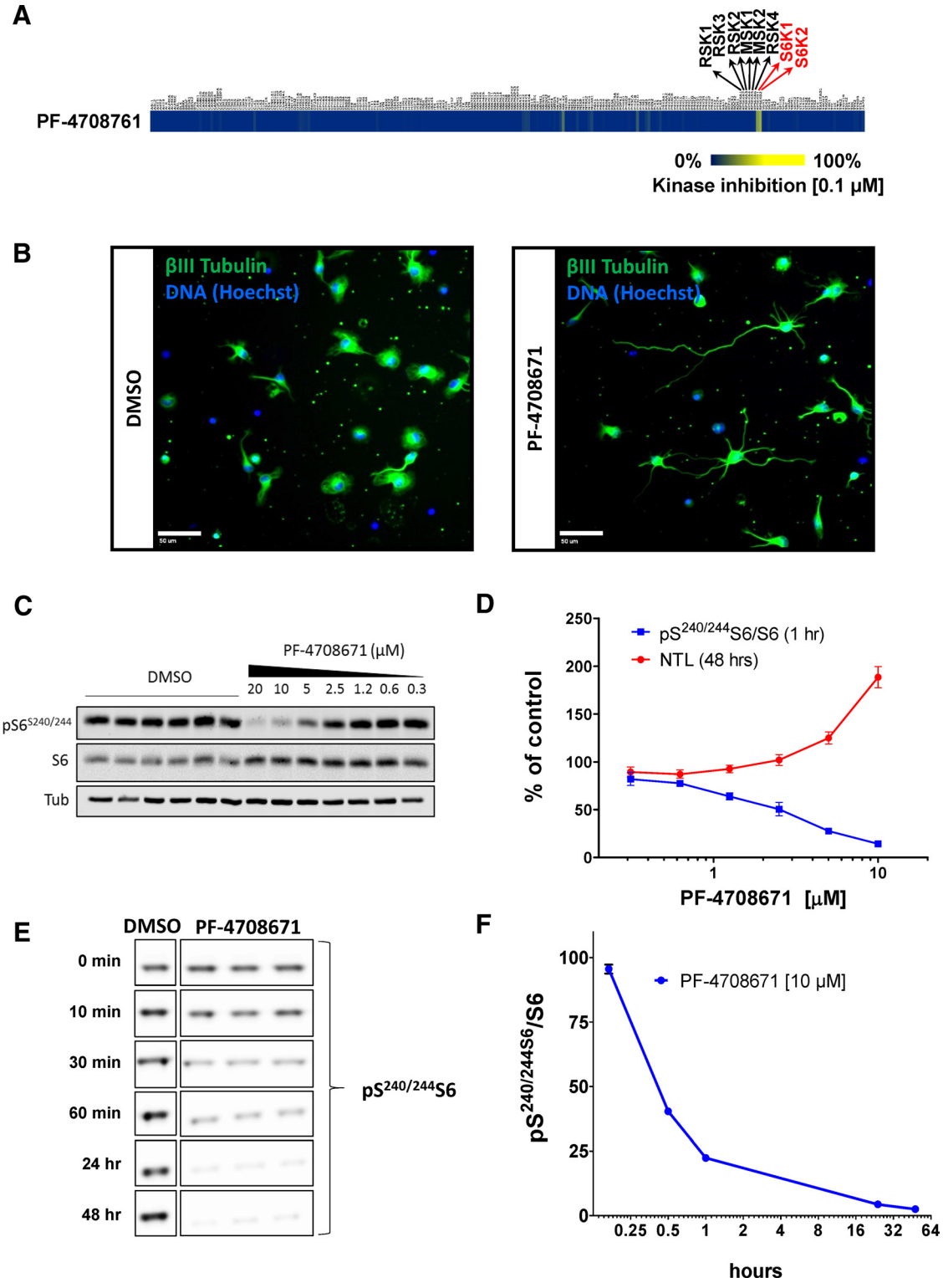

Figure 2. A selective S6K1 inhibitor promotes neurite outgrowth in primary hippocampal neurons. ***A***, in vitro kinase inhibition profiling of PF-4708671 with a panel of 200 kinases (Al-Ali et al., 2015) shows activity against S6K1 and its isoform S6K2, and little to no activity against other kinases, including other members of the RPS6K family of kinases. ***B***, Hippocampal neurons treated with 10 μM PF-4708671 for 48 h (right) show longer neurites than those treated with vehicle (left). Green represents βIII-tubulin immunostaining. Blue represents nuclear stain. Scale bar, 50 μm. ***C***, Western blot of cell lysates from neurons treated for 1 h with PF-4708671 at the indicated concentrations. ***D***, Red circles represent quantification of NTL of neurons treated with PF-4708671 expressed as percentage of DMSO controls. Neurons were treated at the indicated concentrations for 48 h. Data are mean ± SEM. $n = 3$ separate preparations of hippocampal neurons with three experimental replicates for each. Blue squares represent quantification of phospho S6 to pan S6 levels in C expressed as percentage of DMSO control. Data are mean ± SEM. ***E***, Western blot of cell lysates from neurons treated for the indicated times with DMSO or 10 μM PF-4708671. ***F***, Blue squares represent quantification of phospho- to pan-S6 band intensities in ***E*** and expressed as percentage of DMSO control. Data are mean ± SEM. $n = 3$ experimental replicates from a single preparation of primary neurons.

>400-fold selectivity over S6K2 (IC_{50} 0.16 μM vs 65 μM) and >5–60-fold selectivity over RSKs and MSKs. Treating cells with 10 μM PF-4708671 strongly inhibits S6K1 activity with no detectable inhibition of RSKs or MSKs, suggesting that intracellular S6K1 is selectively inhibited at or below that treatment concentration (Pearce et al., 2010a). We treated primary hippocampal neurons with PF-4708671 and found that it induced a large increase in neurite outgrowth relative to DMSO (vehicle) controls, reaching ~200% at 10 μM (Fig. 2*B*). Western blot analysis of lysates from neurons treated for 1 h with PF-4708671 showed a dose-dependent decrease in $S^{240/244}$S6 phosphorylation (Fig. 2*C*,*D*), which was correlated with induction of neurite outgrowth (Fig. 2*D*). With continuous PF-4708671 treatment, S6 phosphorylation remained strongly inhibited for the full duration of the neurite outgrowth assay (Fig. 2*E*,*F*).

SiRNA-mediated knockdown of S6K1 promotes neurite outgrowth

We sought an independent line of evidence that the correlation between S6K1 inhibition and neurite outgrowth can be attributed to S6K1 itself, rather than to pharmacological linkage within the S6 kinase family or another "off target" effect. We previously determined that Accell siRNAs can be used for efficient protein knockdown in cultured hippocampal neurons (Al-Ali et al., 2015). We therefore used Accell siRNAs directed against S6K1 (α-S6K1 siRNA) and found that, by 2 d following transfection, S6K1 protein abundance was reduced by ~60% (Fig. 3*A*,*B*). As expected, this was accompanied by a decrease in S6 phosphorylation at $S^{240/244}$ (Fig. 3*A*,*C*). To investigate the effect of S6K1 knockdown on neurite outgrowth, we treated neurons with α-S6K1 siRNA using the same format as the compound screening assay with two modifications: (1) the number of replicates per condition was increased from 2 to 6 to account for variations inherent to siRNA knockdown experiments; and (2) assay duration was increased from 2 to 5 d to allow time for protein knockdown to take effect. Consistent with the previous inhibitor data, S6K1 knockdown led to a significant increase in neurite total length (NTL) compared with controls (Fig. 3*D*).

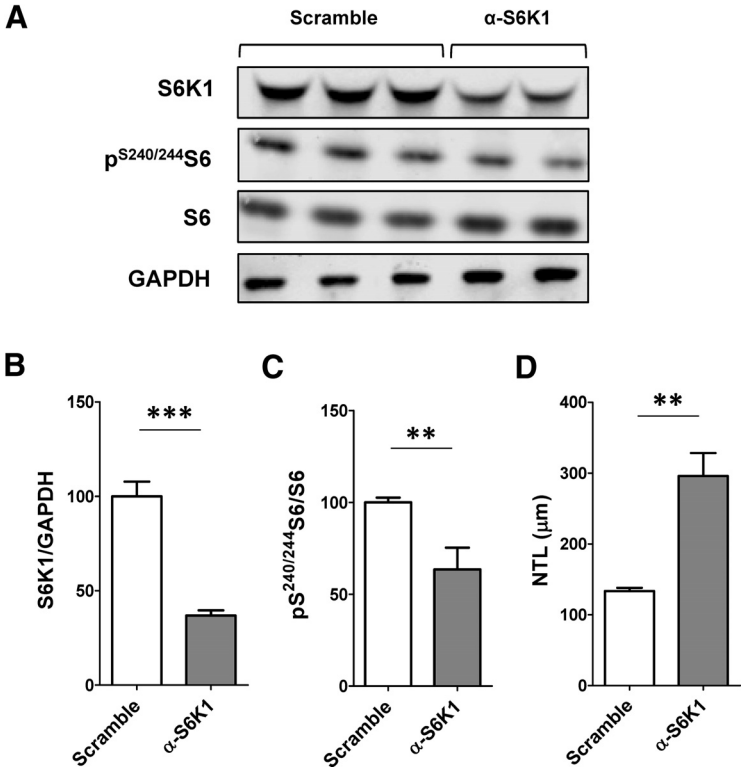

Figure 3. siRNA-mediated knockdown of S6K1 promotes neurite outgrowth in primary hippocampal neurons. ***A***, Western blot of cell lysates (3 d after transfection) from neurons transfected with S6K1-targeting or scrambled siRNAs. ***B***, ***C***, Quantification of ***A*** expressed as percentage of scramble control. Data are mean ± SD. ***D***, Quantification of NTL in neurons transfected for 5 d with α-S6K1 siRNA or scrambled control. Data are mean ± SEM. $n = 6$ experimental replicates from a single preparation of primary neurons. $^{**}p < 0.01$ (Student's *t* test, one-tailed). $^{***}p < 0.001$ (Student's *t* test, one-tailed).

Inhibiting S6K1 in primary neurons induces PI3K signaling and stimulates mTOR activity

Studies in non-neuronal cells have shown that S6K1 inhibits PI3K activity, thus serving as a negative feedback regulator of the PI3K/mTOR pathway (Zoncu et al., 2011; Shimobayashi and Hall, 2014). We therefore investigated the effect of S6K1 inhibition on PI3K/mTOR signaling in neurons. PI3K is recruited to the plasma membrane by a variety of transmembrane receptors (e.g., insulin or growth factor receptors), where it catalyzes the phosphorylation of phosphatidylinositol-4,5-bisphosphate (PIP2) into phosphatidylinositol-3,4,5-trisphosphate (PIP3) (Vivanco and Sawyers, 2002). PIP3 recruits and activates kinases like PDK1 and Akt through pleckstrin homology domains, allowing PDK1 to phosphorylate and activate Akt at T^{308} (Sarbassov et al., 2005). PDK1 also phosphorylates S6K1 at T^{229}; however, this step occurs independently of PIP3 and is therefore not directly regulated by PI3K (Mora et al., 2004). Activated Akt leads to activation of mTOR complex 1 (mTORC1), composed of mTOR and its binding partner Raptor (Zoncu et al., 2011). mTORC1 phosphorylates S6K1 at T^{389}, leading to its activation (Q. Liu et al., 2010, 2011). In addition to mTORC1, mTOR forms a second complex with Rictor, mTOR complex 2 (mTORC2) (Sarbassov et al., 2004). PI3K activity (and PIP3 production) stimulates mTORC2, which phosphorylates Akt at S473 and facilitates its activation by PDK1 (Sarbassov et al., 2005). PTEN, a dual-specificity protein/lipid phosphatase, silences this pathway by hydrolyzing PIP3 into PIP2 (Song et al., 2012).

Treating hippocampal neurons with 10 μM PF-4708671 rapidly inhibited S6K1 activity (S6 phosphorylation at $S^{240/244}$; Fig. 4*A*,*B*, blue line). A simultaneous increase was observed in mTORC1 activity (phosphorylation of S6K1 at T^{389}) (Fig. 4*A*,*C*). Additionally, PF-4708671 treatment increased activities of PDK1 (Akt phosphorylation at its T^{308}) and mTORC2 (Akt phosphorylation at its S^{473}) (Fig. 4*A*,*D*,*E*). In agreement with previous work showing that PDK1 phosphorylation of S6K1 is independent of PI3K (Mora et al., 2004), we did not observe a strong increase in S6K1 T^{229} phosphorylation (Fig. 4*A*). These results demonstrate that inhibiting S6K1 in neurons induces the PI3K pathway and leads to the activation of both mTOR complexes.

Inhibiting both mTOR complexes abolishes PF-4708671's effect on neurite outgrowth

To investigate whether mTOR activity is required for neurite outgrowth promotion by PF-4708671, we used two mTOR inhibitors:

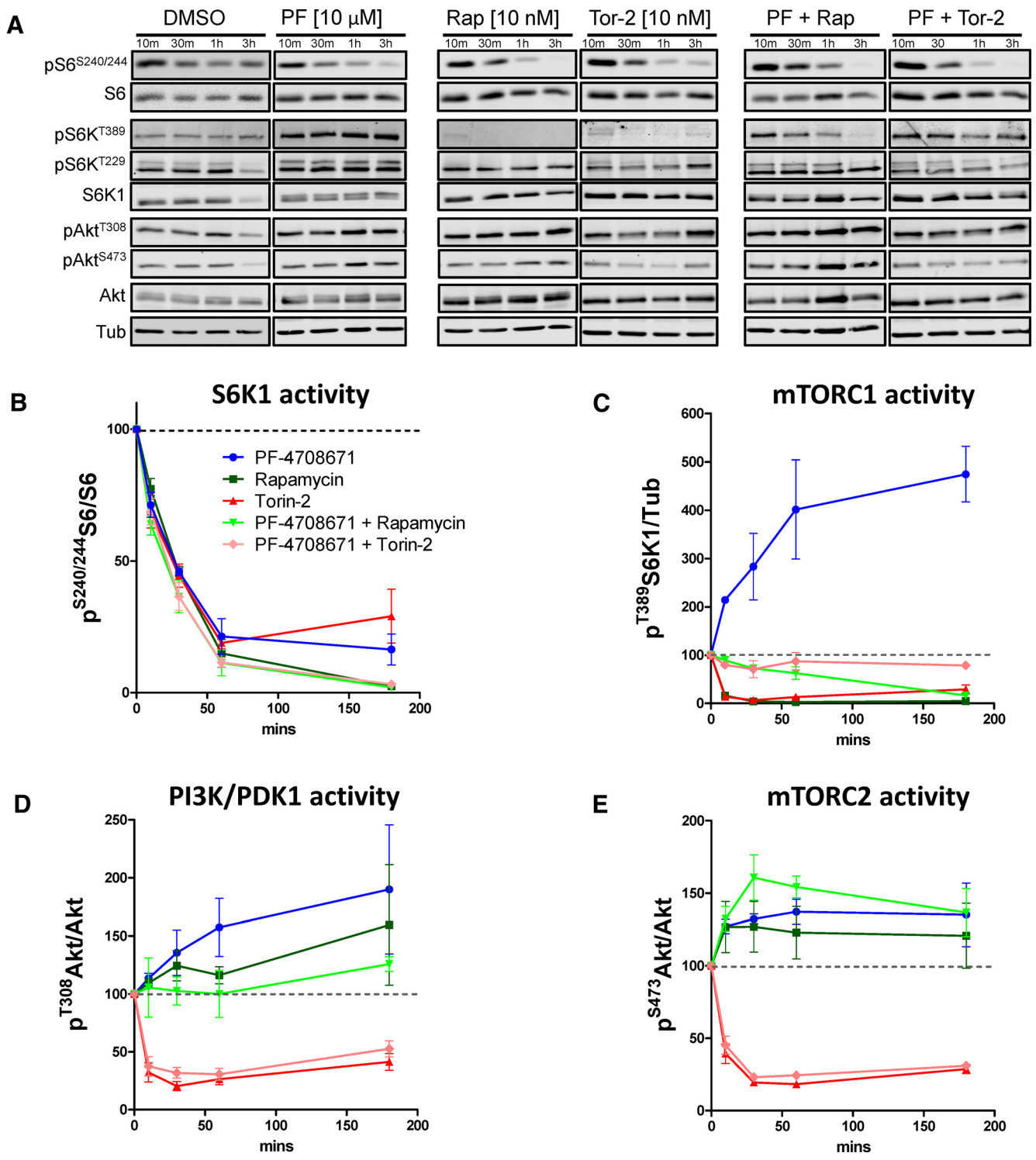

Figure 4. PF-4708671 induces PI3K signaling and stimulates mTORC1 and mTORC2 activities in primary hippocampal neurons. ***A***, Western blot of cell lysates from neurons treated with PF-4708671, rapamycin, and Torin-2, individually or in combination for the indicated times. ***B–E***, Quantification of band intensities in ***A*** expressed as percentage of DMSO controls (dashed lines). Data are mean ± SEM. $n = 3$ experimental replicates from three separate preparations of primary neurons.

rapamycin and Torin-2. Rapamycin is an allosteric, selective, and specific competitive inhibitor of the mTORC1 (Feldman et al., 2009). Torin-2, on the other hand, is an ATP-competitive inhibitor of mTOR kinase, and therefore inhibits both mTORC1 and mTORC2 (Q. Liu et al., 2011). Treating neurons with either rapamycin (10 nM) or Torin-2 (10 nM) inhibited mTORC1, which in turn inhibited S6K1 activity (Fig. 4*A–C*). Whereas rapamycin did not inhibit mTORC2, Torin-2 inhibited it as expected (Fig. 4*A*,*E*). Torin-2 also decreased phosphorylation of Akt at T^{308}, which is likely due to the dependence of PDK1 activity at this site on prior phosphorylation at S^{473} (mTORC2's target site) (Hart and Vogt, 2011).

Treating neurons with either mTOR inhibitor completely inhibited mTORC1 activity, with Torin-2 additionally inhibiting

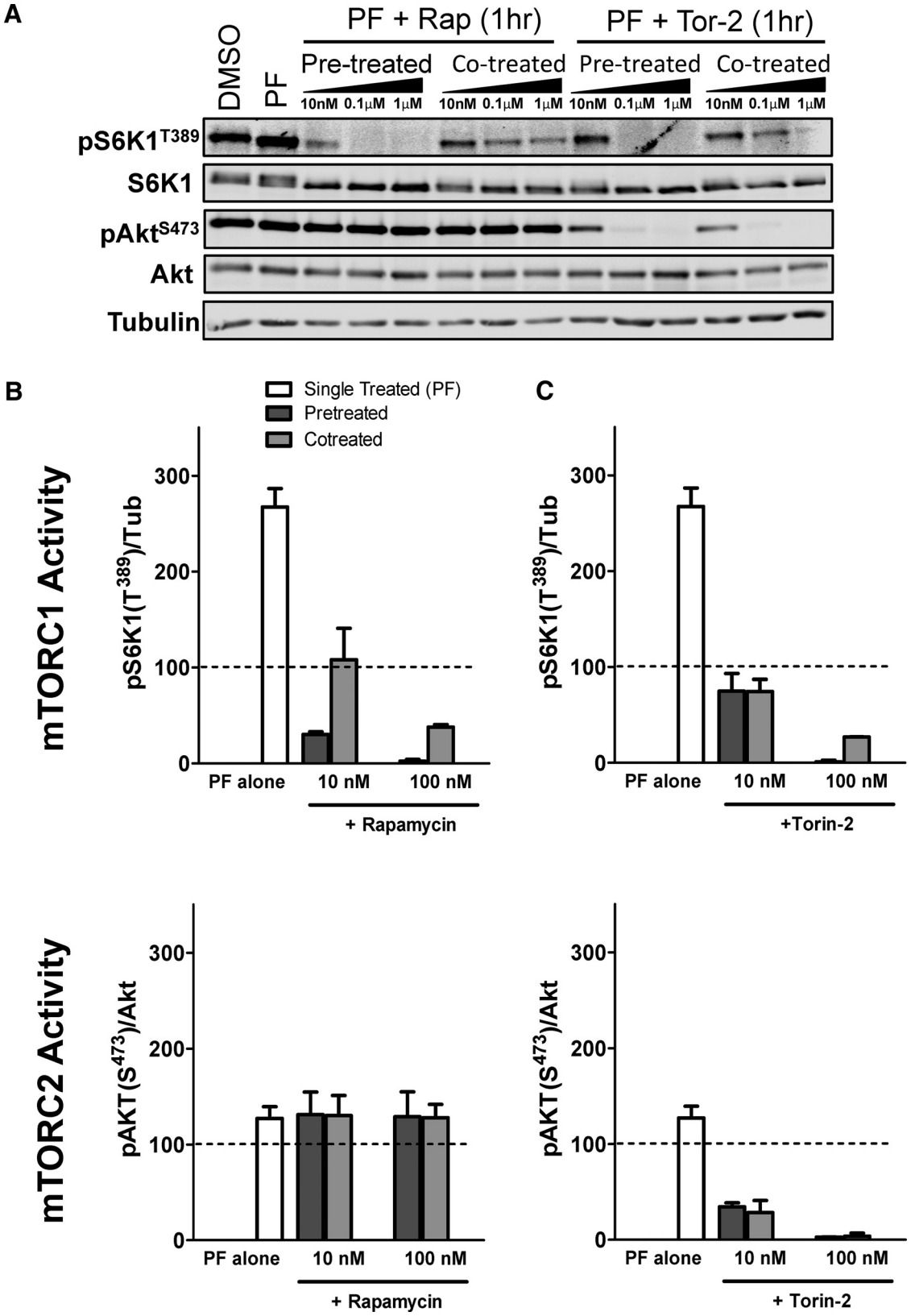

Figure 5. Treatment with mTOR inhibitors counteracts mTORC1 and mTORC2 induction by PF-4708671. ***A***, Western blot of cell lysates from neurons treated with DMSO or PF-4708671, PF-4708671 plus rapamycin (cotreated), PF-4708671 plus Torin-2 (cotreated), rapamycin then PF-4708671 (pretreated), or Torin-2 then PF-4708671 (pretreated) at the indicated concentrations for 1 h. ***B***, ***C***, Quantification of band intensities in ***A*** expressed as percentage of DMSO controls (dashed lines). Data are mean ± SD. $n = 2$ or 3 experimental replicates from a single preparation of primary neurons.

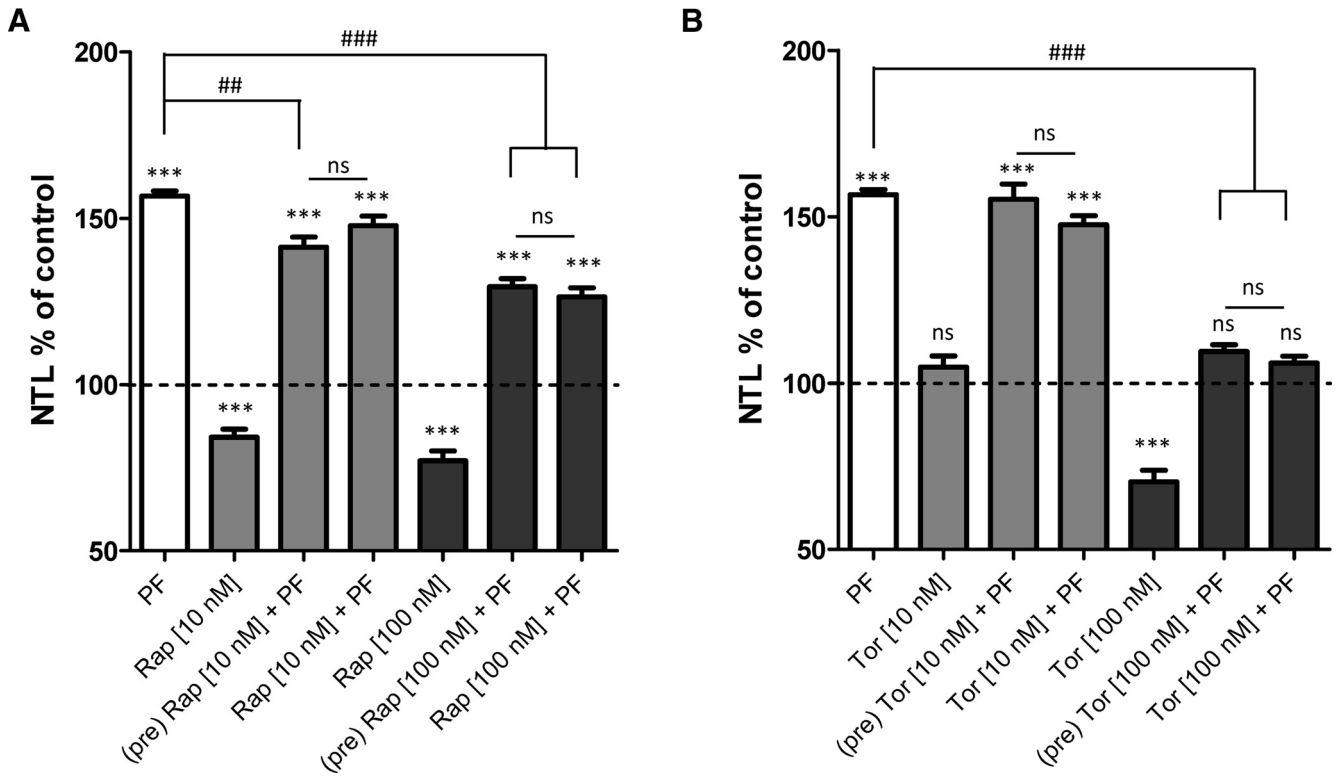

Figure 6. Inhibiting both mTORC1 and mTORC2 abolishes neurite outgrowth promotion by PF-4708671. ***A***, Rapamycin treatment; ***B***, Torin-2 treatment. Quantification of NTL from neurons treated with PF-4708671 alone, rapamycin or Torin2 alone, pretreated with rapamycin or Torin-2 before treatment with PF-4708671, or cotreated with rapamycin or Torin-2 in combination with PF-4708671, expressed as percentage of DMSO controls (dashed lines). Data are mean ± SEM. $n > 15$ technical replicates. $^{*}p < 0.05$, treatment versus DMSO control (one-way ANOVA with Dunnett's multiple comparisons test). $^{**}p < 0.01$, treatment versus DMSO control (one-way ANOVA with Dunnett's multiple comparisons test). $^{***}p < 0.001$, treatment versus DMSO control (one-way ANOVA with Dunnett's multiple comparisons test). $^{\#\#}p < 0.01$ (one-way ANOVA with Tukey's multiple comparisons test). $^{\#\#\#}p < 0.001$ (one-way ANOVA with Tukey's multiple comparisons test).

mTORC2 activity (Fig. 4*A*,*C*). Treating neurons with PF-4708671 together with either mTOR inhibitor prevented the PF-4708671-induced spike in mTORC1 activity (PF-4708671 alone vs PF-4708671 + rapamycin); however, PF-4708671 delayed rapamycin's ability to inhibit mTORC1 activity (PF-4708671 + rapamycin vs rapamycin alone) (Fig. 4*A*,*C*). This suggests that the rapid activation of mTORC1 induced by PF-4708671 counteracts pharmacological inhibition of mTORC1. Thus, to ensure complete inhibition of mTOR during treatment with PF-4708671, we (1) pretreated neurons with the mTOR inhibitors for 1 h before the treatment with PF-4708671 or (2) cotreated with the mTOR inhibitors at a higher concentration (100 nM). Pretreating neurons with 10 nM rapamycin kept mTORC1 activity below control levels even after addition of PF-4708671 (Fig. 5*A*,*B*). Both pretreating and cotreating neurons with 100 nM rapamycin resulted in strong inhibition of mTORC1 that was not counteracted by PF-4708671 (Fig. 5*A*,*B*). Neither pretreating nor cotreating neurons with 10 nM Torin-2 inhibited mTORC1 activity below DMSO control levels after addition of PF-4708671 (Fig. 5*A*,*C*). With 100 nM Torin-2, however, either pretreatment or cotreatment resulted in complete inhibition of mTORC1 and mTORC2, which was not counteracted by PF-4708671 (Fig. 5*A*,*C*). In neurons, therefore, treatment with 100 nM Torin-2 appears to be sufficient for fully inhibiting mTORC1 and mTORC2, and preventing PF-4708671 from countering this inhibition.

We tested the effects of the various treatments in the neurite outgrowth assay. We found that PF-4708671's ability to induce neurite outgrowth was partially lost in conditions where strong inhibition of mTORC1 activity was maintained (pretreatment with 10 nM rapamycin, pretreatment or cotreatment with 100 nM rapamycin; Fig. 6*A*). In conditions where both mTORC1 and mTORC2 were strongly inhibited (pretreatment with 10 nM Torin-2, cotreatment with 100 nM Torin-2), PF-4708671's effect on neurite outgrowth was completely abolished (Fig. 6*B*). These results suggest that mTOR activity is required for connecting the induction in PI3K signaling to the increase in neurite outgrowth, and suggest that mTORC2 has a previously unappreciated role in this process.

Knockdown of S6 protein promotes neurite outgrowth

Dysregulation of S6 phosphorylation is associated with a number of nervous system disorders (Biever et al., 2015). Given the strong correlation between decreased S6 phosphorylation and increased neurite outgrowth in our cells, we sought to explore whether lowering overall levels of S6 can in itself influence neurite outgrowth. We transfected cells with four different siRNAs targeting S6, and compared their effects on both S6 expression and neurite outgrowth. Three of the four S6 targeting oligos showed a marked decrease in S6 mRNA by 24 h following transfection (Fig. 7*A*). The decrease in S6 mRNA levels was correlated with a significant increase in neurite outgrowth in neurons (Fig. 7*B*,*C*), suggesting that decreases in S6 levels (and consequently in levels of phosphorylated S6) are causally associated with promotion of neurite growth. Conversely, neither wild-type S6 nor a phosphorylation-deficient S6 mutant ($Ser^{235,236,240,244,247} \rightarrow Ala$) altered neurite outgrowth when overexpressed in the neurons (data not shown). These data suggest that pS6 levels in the cultured neurons are

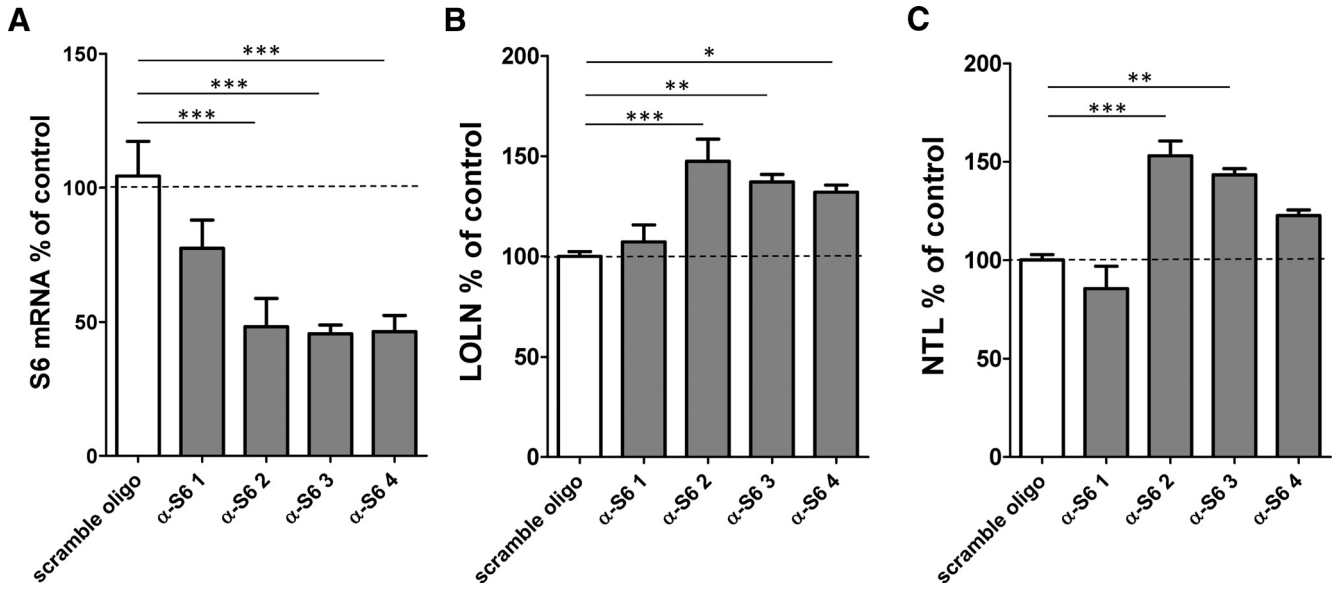

Figure 7. Ribosomal S6 protein knockdown induced neurite outgrowth. ***A***, qPCR quantification of S6 mRNA in neurons treated (24 h) with four different S6-targeting siRNAs or scrambled control (Accell siRNA oligos). α-S6 siRNAs 2–4 significantly reduced S6 mRNA levels. ***B***, ***C***, Quantification of NTL and length of the longest neurite (LOLN) in neurons transfected for 5 d with α-S6 siRNA, expressed as percentage relative to scrambled control (dashed line). α-S6 siRNAs 2–4 significantly increased LOLN, and α-S6 siRNAs 2–3 significantly increased NTL. Data are mean ± SEM. $n = 4$ experimental replicates from a single preparation of primary neurons. *$p < 0.05$ (one-way ANOVA with Dunnett's multiple comparisons test). **$p < 0.01$ (one-way ANOVA with Dunnett's multiple comparisons test). ***$p < 0.001$ (one-way ANOVA with Dunnett's multiple comparisons test).

already at saturating levels, and overexpression sufficient for a dominant negative phenotype is difficult to achieve.

Selective S6K1 inhibitor promotes regeneration of the CST

To assess the effect of S6K1 inhibition on CST axonal regeneration *in vivo*, we injected PF-4708671 bilaterally into sensorimotor cortex (the origin of the CST) immediately after a C5/C6 dorsal spinal cord hemisection (DH) in adult mice (Fig. 8). The compound was injected at three different concentrations: 1, 5, and 10 mM, with 10 μl total volume injected per animal. The anterograde tracer BDA was injected bilaterally into sensorimotor cortex 6 weeks after the surgery, and 7 sagittal/parasagittal sections of the spinal cord spaced 125 μm apart were analyzed (Fig. 9*A*). The middle section was defined as the one that cut through the central canal. The other 6 sections were selected at 125, 250, and 375 μm lateral to the middle section on each side. Figure 9*C–F* shows BDA (axons) and GFAP (astrocytes) double immunostaining in the representative sagittal sections in the highest PF-4708671 dose group. A narrow and delicate lesion gap through the dorsal half of the cord was clearly seen at 8 weeks after DH, ensuring the completeness of the transection of both the dorsal and lateral CST (Fig. 9*B–D*). We found that the highest dose of PF-4708671 promoted considerable regeneration of the BDA-labeled CST axons through and beyond the lesion gap for relatively long distances (>6 mm) (Fig. 9*C–G*). In cross sections of the spinal cord 6–9 mm caudal to the lesion, no labeled CST fibers in the positions of the dorsal and lateral CSTs could be observed (Fig. 9*B*), confirming that both CST projections were completely transected at the lesion site. Importantly, some regenerating CST axons were seen in the gray matter of the spinal cord in these sections, indicating that regenerated CST axons extend for a distance of at least 9 mm beyond the site of dorsal hemisection (Fig. 9*B*). Regeneration of the CST into the distal host spinal cord can be further appreciated by Neurolucida reconstruction (Fig. 9*G*) of a single section shown in Figure 9*F*. High magnification of the lesion area, boxed in Figure 9*C–F*, shows clearly the lesion gap surrounded by reactive astrocytes (Fig. 9*C1–F1*, GFAP, red). Axonal regeneration through the lesion and beyond could be appreciated in these high-magnification images (Fig. 9*C1–F1*, blue arrows). Regenerated axons, after penetrating the lesion gap, grew longitudinally within the gray matter, indicating that the gray matter is more permissive for CST growth than the white matter in this paradigm.

Using BDA and GFAP double immunostaining, we compared regeneration of the CST axons among different groups (Fig. 10). In the DMSO control group, BDA-labeled CST axons stopped at the lesion border with few, if any, axons across the lesion gap (Fig. 10; DMSO control). In each PF-4708671 treatment group, numerous BDA-labeled CST axons were found to regenerate through and beyond the lesion gap and elongate within the gray matter of the distal host spinal cord for considerable distances. Axonal regeneration through the lesion gap in PF-4708671-treated groups could be further appreciated in representative high-magnification images (Fig. 10). Quantification of BDA-labeled CST axons showed that PF-4708671 treatment significantly enhanced CST axonal regeneration compared with the DMSO control (Fig. 10, bottom histogram). The highest dose of PF-4708671 promoted significantly more CST axon regeneration into the 0–0.5 mm zone than the other PF-4708671 doses.

Selective S6K1 inhibitor enhances functional recovery of mice after dorsal hemisection of the cervical spinal cord

Multiple behavioral tests were used to assess forelimb functional recovery after dorsal hemisection of C5/C6 spinal cord: Rotarod, grid-walking, adhesive removal, and single pellet tests. The Rotarod test evaluates forelimb and hindlimb motor coordination and balance. The preinjury baseline test showed no statistically significant differences among starting groups, and the average time on the Rotarod was 81.36 s. The time on the Rotarod remarkably decreased after surgery. At 1 week after surgery, Rotarod performance was significantly better in all groups receiving PF-4708671 compared with the control group (Fig. 11*A*; $p <$

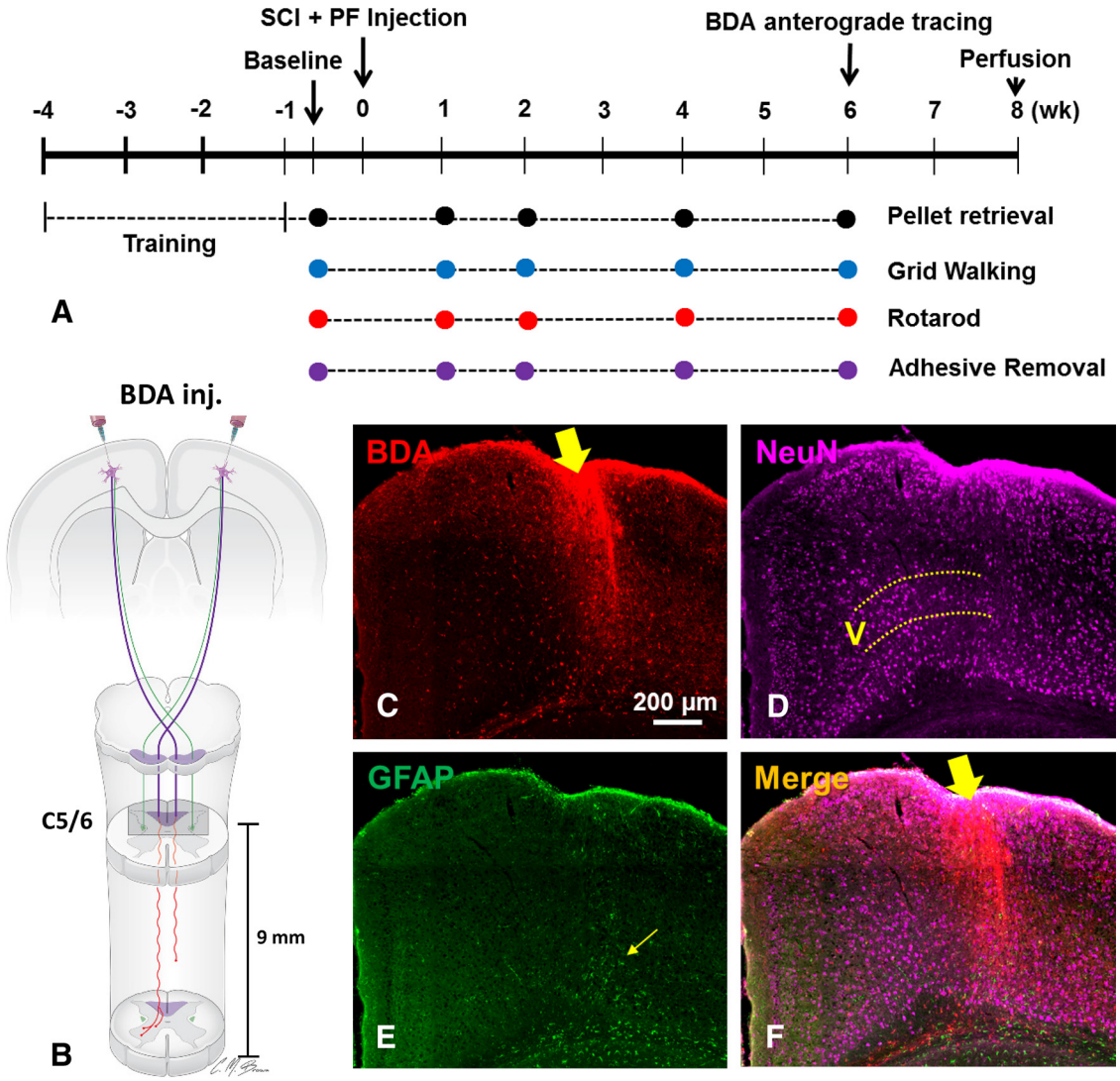

Figure 8. Experimental design of *in vivo* injury model and compound injection. ***A***, Schematic drawing of the timeline, procedures, and behavior assessments. ***B***, Schematic drawing of the tracing of dorsal (purple) and lateral (green) CST from the motor cortex down to the spinal cord. A dorsal hemisection was made at the C5/C6 level that completely transected both the dorsal and lateral CST. In this lesion model, the dorsolateral portion of the lateral funiculus remained intact to facilitate animal survival after the cervical injury. Regeneration of CST axons (red) caudal to the injury were examined up to 9 mm from the lesion site. ***C***, ***D***, After PF-4708671 and BDA injections at two different time points, a coronal section of the brain shows an injection site with BDA labeling (***C***, arrow). Neuronal nuclei (NeuN) staining of the layer V motoneurons showed that the NeuN $^{+}$ motoneurons remained intact at the injection site (***D***). GFAP staining shows that the injections did not trigger strong astrocytic glial responses (arrow) at the site of PF-4708671/BDA injections (***E***). These observations can be further appreciated in a merged image (***F***).

0.01). At 2 weeks after surgery, time on the Rotarod was significantly increased in the 1 mM ($p < 0.01$), 5 mM ($p < 0.001$), and 10 mM PF-4708671 ($p < 0.001$) groups compared with the control group. At 4 weeks and 6 weeks after surgery, only the 10 mM PF-4708671 treatment group showed significantly longer time on the Rotarod compared with the control group ($p < 0.01$). Although there were no statistically significant differences among the three PF-4708671 treatment groups, time on the Rotarod showed a dose-dependent trend. These data suggest that PF-4708671 treatment can improve the forelimb and hindlimb motor coordination and balance of injured mice.

The grid-walking test examines the animal's motor, sensory, and proprioceptive abilities to place the front paws on the rungs of a grid during spontaneous exploration. Before dorsal hemisection, mice walked on the grid with ~99.74% accuracy (forelimb dropped below the grid plane 0.26%). At all observed time points after surgery, the percentage of forelimb drops dramatically increased in all groups compared with the preinjury baseline, especially at 3 d after surgery. There were no statistically significant differences among groups at 3 d or 1 week after surgery (Fig. 11*B*). At 2 weeks after surgery, however, all three PF-4708671 groups showed significantly improved forelimb grid-walking function compared with the control group ($p < 0.001$). At 4 weeks after surgery, the percentage of forelimb drops was significantly decreased in both the 5 mM ($p < 0.05$) and 10 mM ($p < 0.01$) PF-4708671 groups. At 6 weeks after surgery, the percentage of forelimb drops in the 10 mM PF-4708671 group was still significantly lower than the control group ($p < 0.05$). These results indicate that PF-4708671 treatment improves long-term motor, sensory, and proprioceptive abilities after a cervical dorsal hemisection.

The adhesive removal test (Bouet et al., 2009) was used to examine paw and mouth sensitivity (contact time) and dexterity (removal time). At observed time points after surgery, the contact time and removal time in each group were longer than preinjury baselines (Fig. 11*C*,*D*). At 1, 2, and 4 weeks after surgery, both

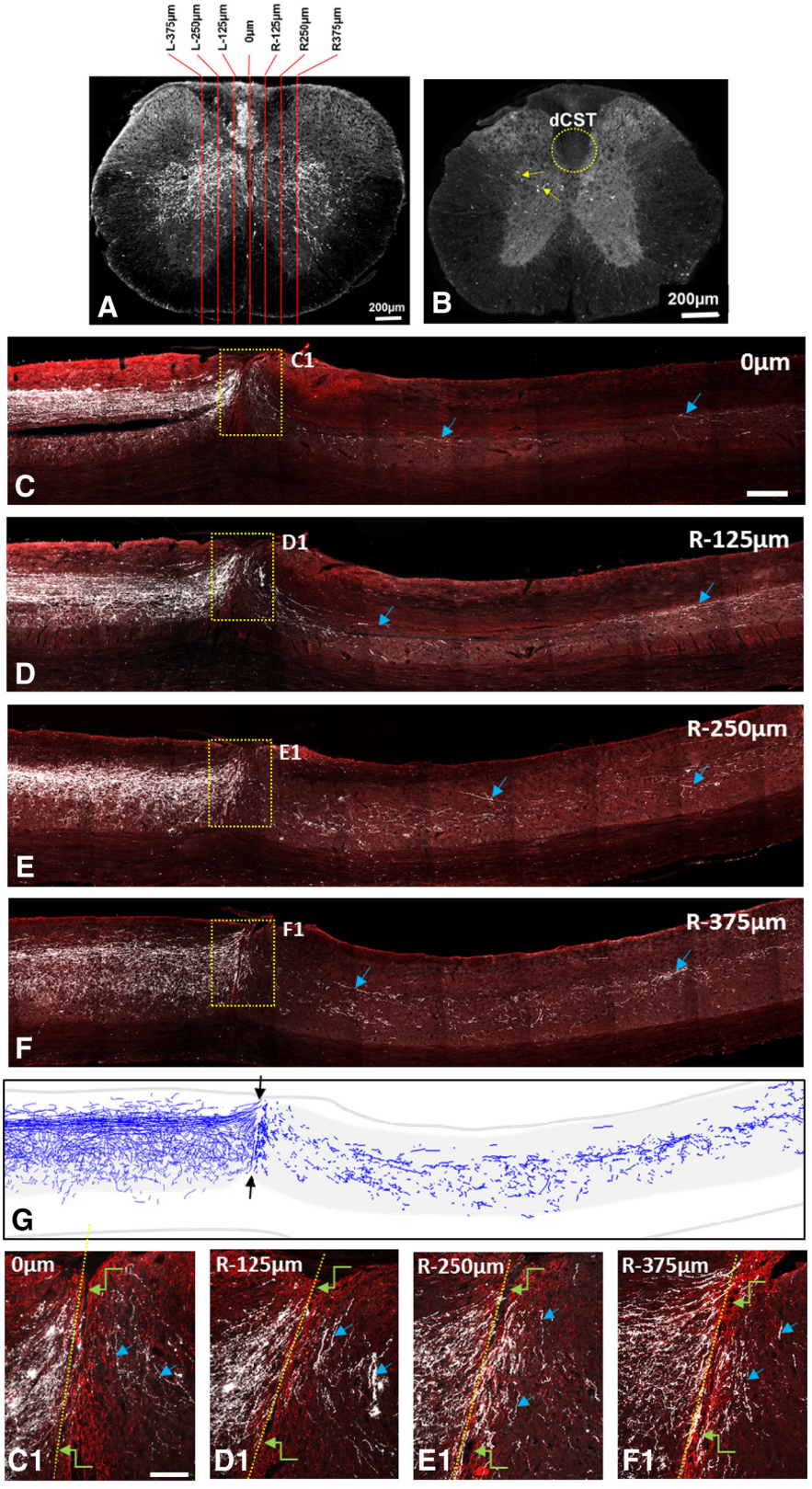

Figure 9. PF-4708671 promoted robust axonal regeneration of the CST through and beyond the dorsal hemisection. ***A***, A cross section of the cervical spinal cord shows bilateral distribution of BDA-labeled main CST tracts (both dorsal and lateral) and their sprouting into the spinal gray matter. Red lines indicate sagittal/parasagittal sections spaced 125 μm apart. ***B***, A cross section of caudal spinal cord segment 9 mm distal to the injury shows a lack of BDA labeling in the dorsal and lateral CSTs, indicating that these tracts were completely transected at C5/C6. Some regenerated CST axons were found in the gray matter of the spinal cord (arrows), indicating that these axons extended for a distance of up to 9 mm beyond the injury site. ***C–F***, Parasagittal sections of the spinal cord, 125 μm apart, from the same animal that received 10 mM PF-4708671 show CST axonal regeneration across and beyond the lesion gap. The regenerated axons elongated within the distal spinal gray matter for considerable distances (blue arrows). ***G***, Neurolucida reconstruction of the single section from ***F*** shows the lesion gap far beyond the main dorsal CST (between two arrows). Varicosities of regenerated CST axons extended within the distal spinal gray matter for considerable distances. ***C1–F1***, High magnification of the lesion area, boxed in ***C–F***, clearly shows the lesion gap (dashed line) surrounded by relatively mild astroglial responses (GFAP-IR, red, zigzag arrows). Axonal regeneration through the narrow lesion gap and beyond could be clearly seen (blue arrows). Notably, the Vibraknife cut produced a complete and deep dorsal hemisection, ensuring the transection of all CST axons at this level. Scale bars: ***A***, ***B***, 200 μm; ***C–F***, 400 μm; ***C1–F1***, 100 μm.

contact time and removal time were significantly shorter in PF-4708671 groups than the control group (Fig. 11*C*,*D*), but there were no significant differences among three PF-4708671 groups. At 6 weeks after surgery, a significantly shorter contact time was observed in the 5 and 10 mM PF-4708671 groups (Fig. 11*C*; $p < 0.05$) compared with controls, and a significantly shorter removal time was observed in the 10 mM PF-4708671 group compared with the control group (Fig. 11*D*; $p < 0.05$).

The single-pellet reaching task is a simple repetitive training protocol used to test the precise and coordinated motor movements of the forelimb. Before surgery, all animals displayed similar daily success rates of pellet retrieval (47.02 ± 1.74%; Fig. 11*E*). Postoperatively, the success rates of mice in all groups was significantly impaired compared with baseline of preinjury. PF-4708671-treated mice showed significant improvement in success rates compared with the control group at 4 and 6 weeks following injury (Fig. 11*E*). Notably, the success rates of mice in the 10 mM PF-4708671 was significantly higher than the 1 mM PF-4708671 group at 6 weeks after injury (Fig. 11*E*; $p < 0.01$). The reach rates in this task were significantly improved in the PF-4708671-treated groups compared with the control group at 1, 2, and 6 weeks after injury (Fig. 11*F*). Grasp rates were significantly higher than control in the 5 and 10 mM PF-4708671 group, but only at 1 week following injury (Fig. 11*G*; $p < 0.05$). Failed reach rates in each of the PF-4708671 groups were significantly lower than the control group at 1, 2, and 6 weeks after injury (Fig. 11*H*). Thus, treatment of the neurons of origin of the CST with PF-4708671 improved behavioral recovery after cervical DH in a dose-dependent manner in a variety of sensorimotor tasks.

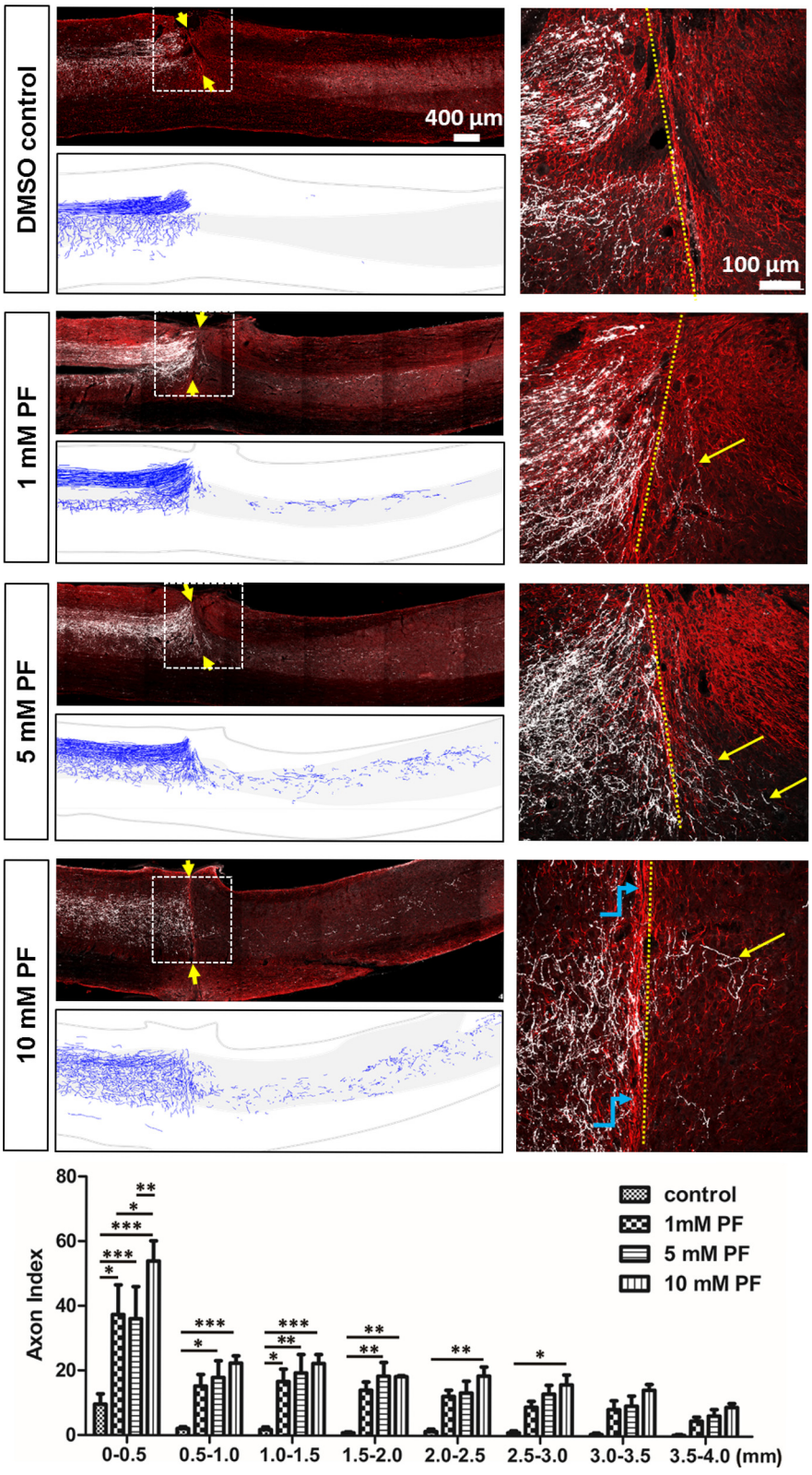

Figure 10. Concentrations of PF-4708671 from 1 to 10 mM increase CST regeneration after a C5/C6 dorsal hemisection. In the DMSO control group, BDA-labeled CST axons stopped at the lesion border (DMSO control). In all three PF-4708671 treatment groups (1, 5, and 10 mM PF-4708671), numerous BDA-labeled CST axons were found to regenerate through and beyond the lesion gap and elongated within the distal spinal cord gray matter for considerable distances. High magnifications of boxed areas in representative sections show CST axonal regeneration across the lesion gap only in the PF-4708671-treated groups. Neurolucida drawings under the same representative images of the four experimental groups show detailed growth patterns of the CST axons across and beyond the lesion gap. Bottom, Quantitative analysis of BDA-labeled CST axons regenerated at different distance zones from the lesion site. In general, PF-4708671 significantly enhanced CST axonal regeneration beyond the lesion gap; 10 mM PF-4708671 promoted higher numbers of regenerative axons at different zones distal to the injury, but a statistically significant difference was only found at the 0–0.5 mm zone compared with the 1 and 5 mM PF-4708671 groups. Data are mean ± SEM. $*p < 0.05$ (two-way repeated-measures ANOVA with Bonferroni post-test). $**p < 0.01$ (two-way repeated-measures ANOVA with Bonferroni post-test). $***p < 0.001$ (two-way repeated-measures ANOVA with Bonferroni post-test).

Discussion

Knockdown or genetic deletion of PTEN promotes substantial axon regeneration in an mTOR-dependent manner, both in the optic nerve and in the CST (Park et al., 2008, 2010; K. Liu et al., 2010; Zukor et al., 2013; Du et al., 2015). It has therefore been suggested that the activity of S6K1, an effector of mTOR, is required for regeneration in this paradigm (Yang et al., 2014). Nevertheless, experimental results on this point are conflicting (Hubert et al., 2014; Yang et al., 2014). In our study, we found that decreased phosphorylation of S6K1's substrate, S6, strongly correlates with promotion of neurite outgrowth in primary neurons treated with a variety of small-molecule kinase inhibitors, and that pharmacological inhibition of S6K1 promotes neurite outgrowth in primary neurons. Activation of PI3K/mTOR signaling, in response to the release of S6K1-mediated negative feedback on this pathway, may be driving the induction of neurite outgrowth. Consistent with this, we observed that inhibiting S6K1 in neurons induced a rapid increase in PI3K signaling and led to the induction of both mTORC1 and mTORC2 activities.

Previous studies on S6K1's role in axon growth/regeneration have led to conflicting conclusions. It is plausible that this is due to the complexity of S6K1 expression and regulation. Overexpressing a native form of S6K1 does not readily yield a catalytically active form of the enzyme (Keshwani et al., 2008). Overexpressing a phosphomimetic mutant kinase (Ma and Blenis, 2009), co-overexpressing an activating kinase (Keshwani et al., 2008), or overexpressing a truncated kinase lacking the autoinhibitory domains (Al-Ali et al., 2007) can result in a fully catalytically active enzyme; however, these alterations may disrupt regulation and substrate specificity (Pearce et al., 2010b), potentially distancing the overexpressed kinase from native biology. We thus chose siRNA-mediated knockdown to obtain independent evidence on S6K1's role in the regulation of neurite outgrowth. Consistent with our

←

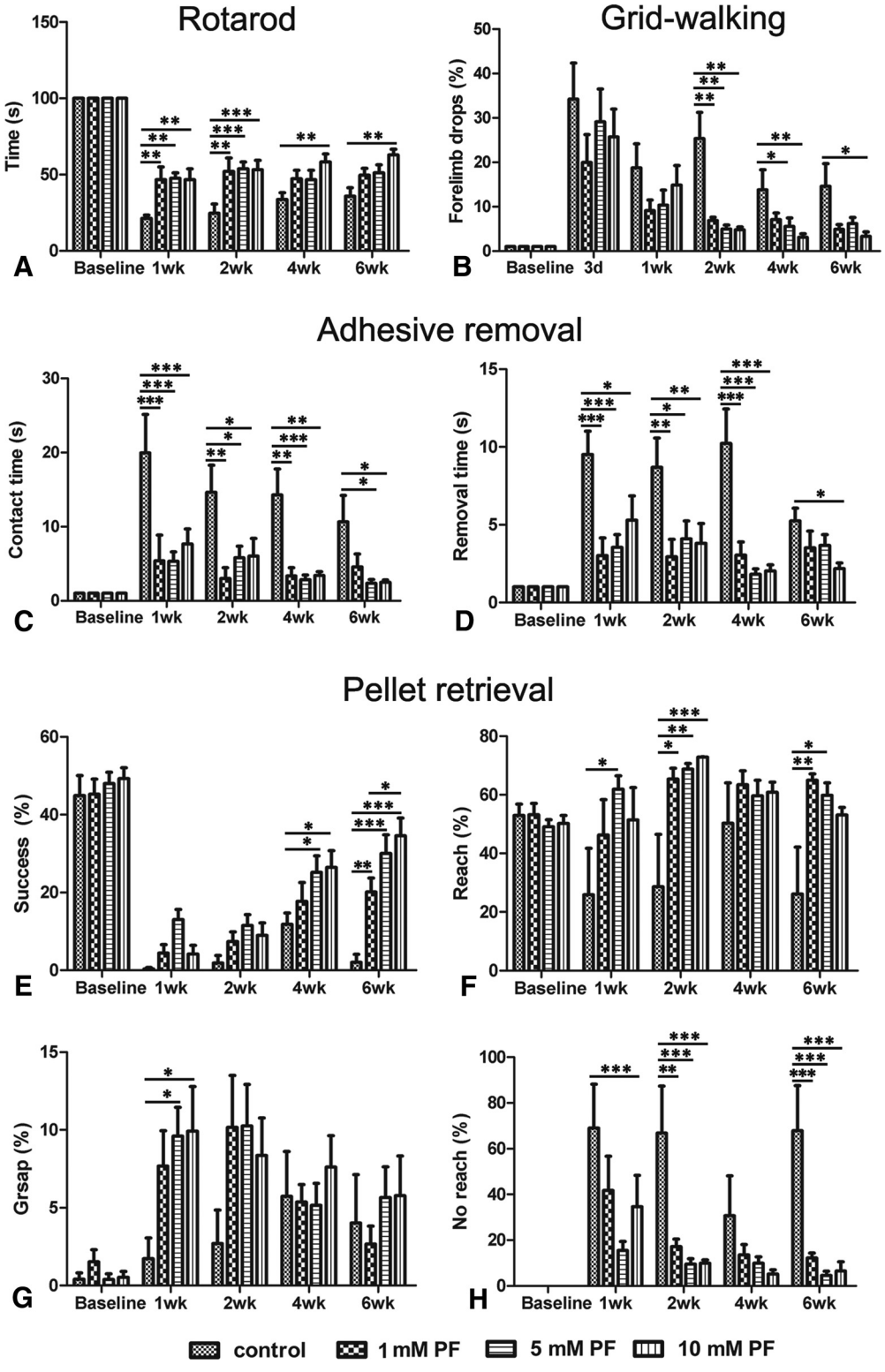

Figure 11. PF-4708671 enhanced functional recoveries of mice after a C5/C6 dorsal hemisection. Rotarod (***A***) forelimb drops at grid-walking (***B***) adhesive removal (***C***, ***D***) and pellet retrieval (***E–H***) show improved behavioral recoveries in groups treated with 1, 5, and 10 mM PF-4708671, compared with the control groups. At one or more time points for several tests, 10 mM PF-4708671 showed significant differences from control when 1 and 5 mM treatments did not (e.g., Rotarod at 4 and 6 weeks). Data are mean ± SEM. *$p < 0.05$ (two-way repeated-measures ANOVA with Bonferroni post-test). **$p < 0.01$ (two-way repeated-measures ANOVA with Bonferroni post-test). ***$p < 0.001$ (two-way repeated-measures ANOVA with Bonferroni post-test).

pharmacological data, we found that knocking down S6K1 promotes neurite outgrowth.

A variety of experimental approaches has led to the conclusion that mTORC1 activation is a key element in the induction of axon growth (Park et al., 2010). We therefore investigated whether mTORC1 activity is required for neurite outgrowth induced by S6K1 inhibition. Indeed, inhibiting mTORC1 with rapamycin reduced, but did not completely abolish, the amount of neurite

outgrowth induced by PF-4708671. Inhibiting both mTORC1 and mTORC2 with Torin-2, on the other hand, completely abrogated PF-4708671's ability to promote neurite growth. Previous studies have shown that the mTORC2 regulates actin polymerization and cytoskeletal dynamics (Jacinto et al., 2004; Angliker and Rüegg, 2013). Mice deficient in mTORC2 exhibit reduced actin polymerization in the hippocampus and present with disrupted LTP and impaired memory (Huang et al., 2013). Our results suggest that mTORC2 may also play a role in neurite outgrowth and axon regeneration within the PI3K/PTEN network. Multiple effectors and interaction partners of mTORC2 are known regulators of axon growth and may be involved in mediating its effects, including the kinases Akt and PKC, and the GTPase Rac1 (Ng et al., 2002; Sivasankaran et al., 2004; Park et al., 2008; Quinn et al., 2008; Oh and Jacinto, 2011).

The strong regulation of neurite growth by manipulation of S6K1 suggests that phosphorylation of S6, S6K1's substrate, is important in neurite outgrowth. Despite the large number of studies using phosphorylation of S6 as a marker for protein translational activity, the biological significance of S6's phosphorylation has remained controversial, suggesting the presence of complex and likely cell-specific regulatory mechanisms (Magnuson et al., 2012; Biever et al., 2015). S6 phosphorylation was originally proposed to be required for the translation of the so-called TOP mRNAs, which encode ribosomal protein and translation factors (Meyuhas and Dreazen, 2009), but was later found to be merely a correlated event (Patursky-Polischuk et al., 2009). We manipulated intracellular levels of S6 to alter availability of the protein for phosphorylation, and found that S6 knockdown induced neurite outgrowth in cultured neurons. Although knocking down S6 is not equivalent to specifically decreasing the availability of phosphorylated S6, it demonstrates that decreasing production of S6 (and presumably, of its phosphorylated form) can promote neurite outgrowth.

In studies of PTEN knockdown or genetic deletion, activation of mTORC1 is consistently correlated with activation of S6K1, and with phosphorylation of ribosomal S6. Consequently, S6 phosphorylation has been used as a marker of mTORC1 activation and, by extension, axon growth ability. Conclusions from these studies, however, are complicated by the fact that some investigators examined S6 phosphorylation sites that are not exclusive to S6K1 (Biever et al., 2015), whereas others have not specified which S6 phosphorylation sites were probed. In this study, we demonstrate that perturbagens that promote neurite outgrowth through inhibition of S6K1 activity can produce both mTOR activation and a reduction in S6 phosphorylation. We therefore propose that the mTOR target site on S6K1, T^{389}S6K1, is a more reliable marker for mTORC1 activation vis-à-vis axon regeneration than is S6 phosphorylation.

Because inhibiting S6K1 can induce neurite growth in cultured neurons, we investigated the effect of S6K1 inhibition on axon regeneration (and on behavioral recovery) *in vivo*, in a dorsal hemisection model of spinal cord injury. Notably, our model produces a precise and definitive anatomical lesion that completely transects the dCST and dlCST (Sivasankaran et al., 2004; Y. Liu et al., 2008; Zhang et al., 2013). Thus, the model can provide clean and definitive anatomical evidence of CST axonal regeneration. We injected PF-4708671 once, bilaterally, into sensorimotor cortex, following a previously established method (Wang et al., 2014). This single injection had a pronounced effect on CST regeneration across and beyond the lesion gap. Previously, a single cortical injection of Gö6976, an inhibitor of PKC and other kinases, was shown to promote CST axonal regeneration and forelimb functional recovery after a C4 dorsal hemisection in adult rats (Wang et al., 2014). It appears that delivering these kinase inhibitors to the cell bodies of the CST neurons is important because Gö6976 delivery to the transected CST axons at the lesion site did not elicit axonal regeneration after a similar injury (Sivasankaran et al., 2004; Wang et al., 2014). Supporting the idea that the CST axons in our model were regenerating, rather than spared, was the fact that caudal to the transection, axons were observed in the gray matter and not in the dorsal or lateral CST tracts. This is the same pattern observed with other treatments that promote CST regeneration, such as PTEN knockout, PTEN-SOCS3 double knockout, or overexpression of VP16-KLF7 or Sox11 (Blackmore et al., 2012; Du et al., 2015; Jin et al., 2015; Wang et al., 2015). Although it is not possible to directly compare experiments done in different laboratories, it is intriguing that the density and distance from the lesion of regenerating CST fibers after a single PF treatment appear to equal or exceed axon growth observed with PTEN knockout, or with overexpression of VP16-KLF7 or Sox11 (Wang et al., 2011; Blackmore et al., 2012; Zukor et al., 2013; Jin et al., 2015). In this context, a single injection of a small-molecule inhibitor provides advantages over these direct manipulations of gene expression because it is convenient and easier to produce and deliver.

CST damage in rodents causes deficits primarily in fine control of the forelimbs, which is required for grasping and holding objects (Anderson et al., 2007; Courtine et al., 2007). We performed a variety of behavioral assessments to investigate the recovery of forelimb function following dorsal spinal hemisection. Using injection of PF-4708671 to inhibit S6K1, we found improvements in functional outcomes for tests of pellet retrieval, grid walking, Rotarod, and adhesive removal, with clear evidence of a dose–response relationship. These tasks measure different aspects of sensorimotor function, suggesting that S6K1 inhibition in corticospinal neurons helps to rebuild the neural network controlling forelimb movements. Because a number of the functional improvements associated with PF-4708671 administration were evident as early as 1 week after injury, the relationship between regeneration of CST axons beyond the injury site and recovery of function may be complex and multifactorial.

The fact that single PF-4708671 injections into sensorimotor cortex allow extensive axon growth beyond a spinal cord lesion raises the possibility that strong inhibition of S6K1 (and activation of mTOR) produces long-term changes in the intrinsic state of the CST neurons. Indeed, activation of the mTOR pathway, in addition to effects on protein synthesis, is known to affect gene transcription by a variety of mechanisms (Laplante and Sabatini, 2013). It may be that treatment of cortical projection neurons with PF-4708671 can lead to sustained changes in transcription factor activity and/or in epigenetic regulation. If so, it would be important to understand the mechanisms underlying these longer-term changes.

Although our data provide specific evidence on S6K1's involvement in regulating axon growth, we cannot rule out a role for S6K2. Under normal conditions, S6K1 and S6K2 have distinct biological roles and subcellular localization patterns (Pardo and Seckl, 2013). However, knockout studies suggest that the two isoforms have overlapping functions, and that S6K2 can partially compensate for the S6K1 deletion (Pende et al., 2004). It will be interesting to investigate whether S6K2 can compensate for S6K1 inhibition in the context of axon growth promotion, and whether simultaneous targeting of both isoforms is required for long-term treatment efficacy.

A potential advantage of targeting S6K1, compared with pharmacological or genetic inhibition of PTEN, is that it can induce mTOR activation and transient increases in axon growth and regeneration, without the potentially tumor-promoting effects of PTEN inactivation (Song et al., 2012). The potential use of S6K1 inhibitors as drugs for neurodegeneration is further encouraged by the fact that S6K1 inhibitors are in Phase III clinical trials for other nononcological indications, such as liver cirrhosis and insulin resistance (Hameed and Terrault, 2016). Our results, together, implicate S6K1 as a potential target for drugs that improve axon regeneration and functional recovery following CNS injury.

References

Al-Ali H, Ragan TJ, Gao X, Harris TK (2007) Reconstitution of modular PDK1 functions on trans-splicing of the regulatory PH and catalytic kinase domains. Bioconjug Chem 18:1294–1302. CrossRef Medline

Al-Ali H, Blackmore M, Bixby JL, Lemmon VP (2013a) High content screening with primary neurons. In: Assay guidance manual. Bethesda, MD: Eli Lilly.

Al-Ali H, Schürer SC, Lemmon VP, Bixby JL (2013b) Chemical interrogation of the neuronal kinome using a primary cell-based screening assay. ACS Chem Biol 8:1027–1036. CrossRef Medline

Al-Ali H, Lee DH, Danzi MC, Nassif H, Gautam P, Wennerberg K, Zuercher B, Drewry DH, Lee JK, Lemmon VP, Bixby JL (2015) Rational polypharmacology: systematically identifying and engaging multiple drug targets to promote axon growth. ACS Chem Biol 10:1939–1951. CrossRef Medline

Al-Ali H, Beckerman SR, Bixby JL, Lemmon VP (2017) In vitro models of axon regeneration. Exp Neurol 287:423–434. CrossRef Medline

Anderson KD, Gunawan A, Steward O (2007) Spinal pathways involved in the control of forelimb motor function in rats. Exp Neurol 206:318–331. CrossRef Medline

Angliker N, Rüegg MA (2013) In vivo evidence for mTORC2-mediated actin cytoskeleton rearrangement in neurons. Bioarchitecture 3:113–118. CrossRef Medline

Biever A, Valjent E, Puighermanal E (2015) Ribosomal protein S6 phosphorylation in the nervous system: from regulation to function. Front Mol Neurosci 8:75. CrossRef Medline

Blackmore MG, Wang Z, Lerch JK, Motti D, Zhang YP, Shields CB, Lee JK, Goldberg JL, Lemmon VP, Bixby JL (2012) Krüppel-like Factor 7 engineered for transcriptional activation promotes axon regeneration in the adult corticospinal tract. Proc Natl Acad Sci U|S|A 109:7517–7522. CrossRef Medline

Bouet V, Boulouard M, Toutain J, Divoux D, Bernaudin M, Schumann-Bard P, Freret T (2009) The adhesive removal test: a sensitive method to assess sensorimotor deficits in mice. Nat Protoc 4:1560–1564. CrossRef Medline

Buchser WJ, Slepak TI, Gutierrez-Arenas O, Bixby JL, Lemmon VP (2010) Kinase/phosphatase overexpression reveals pathways regulating hippocampal neuron morphology. Mol Syst Biol 6:391. CrossRef Medline

Chen CC, Gilmore A, Zuo Y (2014) Study motor skill learning by single-pellet reaching tasks in mice. J Vis Exp 85:e51238-e51238. CrossRef Medline

Courtine G, Bunge MB, Fawcett JW, Grossman RG, Kaas JH, Lemon R, Maier I, Martin J, Nudo RJ, Ramon-Cueto A, Rouiller EM, Schnell L, Wannier T, Schwab ME, Edgerton VR (2007) Can experiments in nonhuman primates expedite the translation of treatments for spinal cord injury in humans? Nat Med 13:561–566. CrossRef Medline

Du K, Zheng S, Zhang Q, Li S, Gao X, Wang J, Jiang L, Liu K (2015) Pten deletion promotes regrowth of corticospinal tract axons 1 year after spinal cord injury. J Neurosci 35:9754–9763. CrossRef Medline

Feldman ME, Apsel B, Uotila A, Loewith R, Knight ZA, Ruggero D, Shokat KM (2009) Active-site inhibitors of mTOR target rapamycin-resistant outputs of mTORC1 and mTORC2. PLoS Biol 7:e38. CrossRef Medline

Fischer M, Pereira PM, Holtmann B, Simon CM, Hanauer A, Heisenberg M, Sendtner M (2009) P90 Ribosomal s6 kinase 2 negatively regulates axon growth in motoneurons. Mol Cell Neurosci 42:134–141. CrossRef Medline

Hameed B, Terrault N (2016) Emerging therapies for nonalcoholic fatty liver disease. Clin Liver Dis 20:365–385. CrossRef Medline

Hart JR, Vogt PK (2011) Phosphorylation of AKT: a mutational analysis. Oncotarget 2:467–476. CrossRef Medline

Huang W, Zhu PJ, Zhang S, Zhou H, Stoica L, Galiano M, Krnjević K, Roman G, Costa-Mattioli M (2013) mTORC2 controls actin polymerization required for consolidation of long-term memory. Nat Neurosci 16:441–448. CrossRef Medline

Hubert T, Wu Z, Chisholm AD, Jin Y (2014) S6 kinase inhibits intrinsic axon regeneration capacity via AMP kinase in *Caenorhabditis elegans*. J Neurosci 34:758–763. CrossRef Medline

Jacinto E, Loewith R, Schmidt A, Lin S, Rüegg MA, Hall A, Hall MN (2004) Mammalian TOR complex 2 controls the actin cytoskeleton and is rapamycin insensitive. Nat Cell Biol 6:1122–1128. CrossRef Medline

Jin D, Liu Y, Sun F, Wang X, Liu X, He Z (2015) Restoration of skilled locomotion by sprouting corticospinal axons induced by co-deletion of PTEN and SOCS3. Nat Commun 6:8074. CrossRef Medline

Keshwani MM, Ross DB, Ragan TJ, Harris TK (2008) Baculovirus-mediated expression, purification, and characterization of a fully activated catalytic kinase domain construct of the 70 kDa 40S ribosomal protein S6 kinase-1 alphaII isoform (S6K1alphaII). Protein Expr Purif 58:32–41. CrossRef Medline

Laplante M, Sabatini DM (2013) Regulation of mTORC1 and its impact on gene expression at a glance. J Cell Sci 126:1713–1719. CrossRef Medline

Liu K, Lu Y, Lee JK, Samara R, Willenberg R, Sears-Kraxberger I, Tedeschi A, Park KK, Jin D, Cai B, Xu B, Connolly L, Steward O, Zheng B, He Z (2010) PTEN deletion enhances the regenerative ability of adult corticospinal neurons. Nat Neurosci 13:1075–1081. CrossRef Medline

Liu NK, Zhang YP, O'Connor J, Gianaris A, Oakes E, Lu QB, Verhovshek T, Walker CL, Shields CB, Xu XM (2013) A bilateral head injury that shows graded brain damage and behavioral deficits in adult mice. Brain Res 1499:121–128. CrossRef Medline

Liu Q, Chang JW, Wang J, Kang SA, Thoreen CC, Markhard A, Hur W, Zhang J, Sim T, Sabatini DM, Gray NS (2010) Discovery of 1-(4-(4-propionylpiperazin-1-yl)-3-(trifluoromethyl)phenyl)-9-(quinolin-3-yl)benzo[h][1,6]naphthyridin-2(1H)-one as a highly potent, selective mammalian target of rapamycin (mTOR) inhibitor for the treatment of cancer. J Med Chem 53:7146–7155. CrossRef Medline

Liu Q, Wang J, Kang SA, Thoreen CC, Hur W, Ahmed T, Sabatini DM, Gray NS (2011) Discovery of 9-(6-aminopyridin-3-yl)-1-(3-(trifluoromethyl)phenyl)benzo[h][1,6]naphthyridin-2(1H)-one (Torin2) as a potent, selective, and orally available mammalian target of rapamycin (mTOR) inhibitor for treatment of cancer. J Med Chem 54:1473–1480. CrossRef Medline

Liu Y, Wang X, Lu CC, Kerman R, Steward O, Xu XM, Zou Y (2008) Repulsive Wnt signaling inhibits axon regeneration after CNS injury. J Neurosci 28:8376–8382. CrossRef Medline

Loh SH, Francescut L, Lingor P, Bähr M, Nicotera P (2008) Identification of new kinase clusters required for neurite outgrowth and retraction by a loss-of-function RNA interference screen. Cell Death Differ 15:283–298. CrossRef Medline

Ma XM, Blenis J (2009) Molecular mechanisms of mTOR-mediated translational control. Nat Rev Mol Cell Biol 10:307–318. CrossRef Medline

Magnuson B, Ekim B, Fingar DC (2012) Regulation and function of ribosomal protein S6 kinase (S6K) within mTOR signalling networks. Biochem J 441:1–21. CrossRef Medline

Meyuhas O (2015) Ribosomal protein S6 phosphorylation: four decades of research. Int Rev Cell Mol Biol 320:41–73. CrossRef Medline

Meyuhas O, Dreazen A (2009) Ribosomal protein S6 kinase from TOP mRNAs to cell size. Prog Mol Biol Transl Sci 90:109–153. CrossRef Medline

Mora A, Komander D, van Aalten DM, Alessi DR (2004) PDK1, the master regulator of AGC kinase signal transduction. Semin Cell Dev Biol 15:161–170. CrossRef Medline

Ng J, Nardine T, Harms M, Tzu J, Goldstein A, Sun Y, Dietzl G, Dickson BJ, Luo L (2002) Rac GTPases control axon growth, guidance and branching. Nature 416:442–447. CrossRef Medline

Oh WJ, Jacinto E (2011) mTOR complex 2 signaling and functions. Cell Cycle 10:2305–2316. CrossRef Medline

Pardo OE, Seckl MJ (2013) S6K2: the neglected S6 kinase family member. Front Oncol 3:191. CrossRef Medline

Park KK, Liu K, Hu Y, Smith PD, Wang C, Cai B, Xu B, Connolly L, Kramvis I, Sahin M, He Z (2008) Promoting axon regeneration in the adult CNS by modulation of the PTEN/mTOR pathway. Science 322:963–966. CrossRef Medline

Park KK, Liu K, Hu Y, Kanter JL, He Z (2010) PTEN/mTOR and axon regeneration. Exp Neurol 223:45–50. CrossRef Medline

Patursky-Polischuk I, Stolovich-Rain M, Hausner-Hanochi M, Kasir J, Cybulski N, Avruch J, Rüegg MA, Hall MN, Meyuhas O (2009) The TSC-mTOR pathway mediates translational activation of TOP mRNAs by insulin largely in a raptor- or rictor-independent manner. Mol Cell Biol 29:640–649. CrossRef Medline

Pearce LR, Alton GR, Richter DT, Kath JC, Lingardo L, Chapman J, Hwang C, Alessi DR (2010a) Characterization of PF-4708671, a novel and highly specific inhibitor of p70 ribosomal S6 kinase (S6K1). Biochem J 431:245–255. CrossRef Medline

Pearce LR, Komander D, Alessi DR (2010b) The nuts and bolts of AGC protein kinases. Nat Rev Mol Cell Biol 11:9–22. CrossRef Medline

Pende M, Um SH, Mieulet V, Sticker M, Goss VL, Mestan J, Mueller M, Fumagalli S, Kozma SC, Thomas G (2004) S6K1(−/−)/S6K2(−/−) mice exhibit perinatal lethality and rapamycin-sensitive 5′-terminal oligopyrimidine mRNA translation and reveal a mitogen-activated protein kinase-dependent S6 kinase pathway. Mol Cell Biol 24:3112–3124. CrossRef Medline

Quinn CC, Pfeil DS, Wadsworth WG (2008) CED-10/Rac1 mediates axon guidance by regulating the asymmetric distribution of MIG-10/lamellipodin. Curr Biol 18:808–813. CrossRef Medline

Sarbassov DD, Ali SM, Kim DH, Guertin DA, Latek RR, Erdjument-Bromage H, Tempst P, Sabatini DM (2004) Rictor, a novel binding partner of mTOR, defines a rapamycin-insensitive and raptor-independent pathway that regulates the cytoskeleton. Curr Biol 14:1296–1302. CrossRef Medline

Sarbassov DD, Guertin DA, Ali SM, Sabatini DM (2005) Phosphorylation and regulation of Akt/PKB by the rictor-mTOR complex. Science 307:1098–1101. CrossRef Medline

Shimobayashi M, Hall MN (2014) Making new contacts: the mTOR network in metabolism and signalling crosstalk. Nat Rev Mol Cell Biol 15:155–162. CrossRef Medline

Sivasankaran R, Pei J, Wang KC, Zhang YP, Shields CB, Xu XM, He Z (2004) PKC mediates inhibitory effects of myelin and chondroitin sulfate proteoglycans on axonal regeneration. Nat Neurosci 7:261–268. CrossRef Medline

Song MS, Salmena L, Pandolfi PP (2012) The functions and regulation of the PTEN tumour suppressor. Nat Rev Mol Cell Biol 13:283–296. CrossRef Medline

Um SH, Frigerio F, Watanabe M, Picard F, Joaquin M, Sticker M, Fumagalli S, Allegrini PR, Kozma SC, Auwerx J, Thomas G (2004) Absence of S6K1 protects against age- and diet-induced obesity while enhancing insulin sensitivity. Nature 431:200–205. CrossRef Medline

Vivanco I, Sawyers CL (2002) The phosphatidylinositol 3-kinase AKT pathway in human cancer. Nat Rev Cancer 2:489–501. CrossRef Medline

Wang D, Ichiyama RM, Zhao R, Andrews MR, Fawcett JW (2011) Chondroitinase combined with rehabilitation promotes recovery of forelimb function in rats with chronic spinal cord injury. J Neurosci 31:9332–9344. CrossRef Medline

Wang X, Hu J, She Y, Smith GM, Xu XM (2014) Cortical PKC inhibition promotes axonal regeneration of the corticospinal tract and forelimb functional recovery after cervical dorsal spinal hemisection in adult rats. Cereb Cortex 24:3069–3079. CrossRef Medline

Wang Z, Reynolds A, Kirry A, Nienhaus C, Blackmore MG (2015) Overexpression of Sox11 promotes corticospinal tract regeneration after spinal injury while interfering with functional recovery. J Neurosci 35:3139–3145. CrossRef Medline

Yang L, Miao L, Liang F, Huang H, Teng X, Li S, Nuriddinov J, Selzer ME, Hu Y (2014) The mTORC1 effectors S6K1 and 4E-BP play different roles in CNS axon regeneration. Nat Commun 5:5416. CrossRef Medline

Zerhouni E (2004) PTEN delection enhances the regenerative ability of adult corticospinal neurons. Science 13:1075–1081.

Zhang YP, Walker MJ, Shields LB, Wang X, Walker CL, Xu XM, Shields CB (2013) Controlled cervical laceration injury in mice. J Vis Exp 75:e50030. CrossRef Medline

Zoncu R, Efeyan A, Sabatini DM (2011) mTOR: from growth signal integration to cancer, diabetes and ageing. Nat Rev Mol Cell Biol 12:21–35. CrossRef Medline

Zukor K, Belin S, Wang C, Keelan N, Wang X, He Z (2013) Short hairpin RNA against PTEN enhances regenerative growth of corticospinal tract axons after spinal cord injury. J Neurosci 33:15350–15361. CrossRef Medline